Hourly measurement of PM$_{2.5}$-bound nonpolar organic compounds in Shanghai: Characteristics, sources and health risk assessment

Kun Zhang [a,b,1], Liumei Yang [a,b,1], Qing Li [a,b], Rui Li [a,b], Dongping Zhang [a,b], Wen Xu [c], Jialiang Feng [a,b], Qiongqiong Wang [d], Wu Wang [a,b], Ling Huang [a,b], Elly Arukulem Yaluk [a,b], Yangjun Wang [a,b], Jian Zhen Yu [d,e], Li Li [a,b,*]

[a] School of Environmental and Chemical Engineering, Shanghai University, Shanghai, China
[b] Key Laboratory of Organic Compound Pollution Control Engineering (MOE), Shanghai University, Shanghai, China
[c] Aerodyne Research Inc., Billerica, MA, USA
[d] Department of Chemistry, Hong Kong University of Science & Technology, Hong Kong, China
[e] Division of Environment & Sustainability, Hong Kong University of Science & Technology, Hong Kong, China

HIGHLIGHTS

- Hourly ambient PM$_{2.5}$-bound NPOCs are quantified and analyzed based on TAG measurement in Shanghai.
- PSCF results indicate that alkanes are mainly from southeast China, while PAHs are mainly from northeastern China.
- Hourly variation of NPOC sources was obtained by PMF model.
- Health risk of PAHs is mostly below the acceptable level during summer and autumn season in Shanghai.

GRAPHICAL ABSTRACT
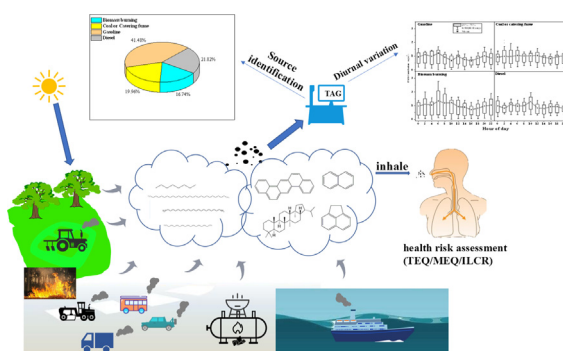
ARTICLE INFO

ABSTRACT

Fine particulate matter (PM$_{2.5}$)-bound nonpolar organic compounds (NPOCs), including polycyclic aromatic hydrocarbons (PAHs) and alkanes, are commonly used as typical molecular markers for detailed source identification. Online thermal desorption aerosol gas chromatography–mass spectrometry (TAG) system can obtain ambient data with hourly resolution, which is of great importance for investigating the diurnal characteristics and refined source identification of NPOCs. From June to October 2020, hourly ambient aerosol samples were collected and analyzed to investigate the characteristics and sources of 14 PAHs and 15 alkanes (C$_{21}$-C$_{35}$) in PM$_{2.5}$ using TAG at a suburban site of Baoshan district in Shanghai, China. The average concentration of summed PAHs and alkanes during the sampling period was 1.27 ± 1.4 ng/m^3 and 8.87 ± 3.46 ng/m^3, respectively, in which Benzo[b]fluoranthene (BbF), Benzo[ghi]perylene (BghiP) and Indeno[1,2,3-cd]pyrene (IcdP) are the dominant PAHs species, with n-Heptacosane (C27), n-Nonacosane (C29) and n-Hentriacontane (C31) being the most abundant n-alkane species. Carbon preference index (CPI) and carbon maximum (C$_{max}$) number indicated that the sources of alkanes shifted from biogenic-oriented (such as plant wax) in the summer to anthropogenic-dominated (such as fossil fuels) in the autumn. Results from trajectory cluster analysis and potential source contribution function (PSCF) modeling showed that alkanes were mainly from the middle and lower reaches of the Yangtze River Plain including Anhui, Jiangxi, and Zhejiang provinces, while PAHs were mainly from northeastern China. Positive Matrix Factorization (PMF) model results indicated that gasoline (41.48%) and diesel (21.82%)

---

* Corresponding author at: School of Environmental and Chemical Engineering, Shanghai University, Shanghai, China.
  E-mail address: Lily@shu.edu.cn (L. Li).
[1] These authors contribute equally to this work.

were the two major sources of $PM_{2.5}$-bound PAHs in summer and fall of 2020 in Shanghai, followed by coal consumption or catering (19.96%) and biomass burning (16.74%). Diurnal variation of PAHs sources resolved by PMF showed characteristic features consistent with the corresponding anthropogenic activities. For example, gasoline vehicle exhaust showed higher concentrations during traffic rush hours; while coal consumption or catering presented higher concentrations during lunch times from 10:00 to 12:00. In addition, the TAG data coupling with PMF also can be capable for source appointment of short-duration episodes. Health risk assessment showed that adult women were at greater lifetime cancer risk (ILCR) than people in other age groups, and people may subject to higher health risks at morning and night time. This work demonstrates that hourly NPOCs measured by TAG are uniquely specific on refined source identification and investigation into the characteristics of diurnal variations.

1. Introduction

Fine particulate matter ($PM_{2.5}$) is relevant to global climate forcing (Sun et al., 2019), atmospheric visibility (Liu et al., 2012), biogeochemical cycle and activation of cloud condensation nuclei (CCN) (Andreae and Rosenfeld, 2008). In addition, $PM_{2.5}$ exhibits adverse effects on human health by spreading allergies and contagious ailments of respiration, cardiovascular and reproductive systems (Sachdeva and Attri, 2008). According to previous studies, organic aerosol (OA), composing of primary organic aerosol (POA) and secondary organic aerosol (SOA), account for 20%–80% of $PM_{2.5}$ (He et al., 2020; Zhang et al., 2007). Among the thousands of organic compounds in OA, some specific compounds have been used as markers to identify specific sources of organic aerosols. The organic molecular tracers used in source apportionment studies are generally divided into two categories: polar organic compounds (POCs) and nonpolar organic compounds (NPOCs). NPOCs have been widely studied due to their complexity of sources. Among NPOCs, alkanes (>C12, same below), hopanes, steranes and PAHs are commonly used for source apportionment analysis (Wang et al., 2016b). N-alkanes are relatively stable and high concentrations of n-alkanes were frequently observed in urban regions due to anthropogenic or biogenic emissions (Kotianova et al., 2008). Hopanes can serve as a unique tracer for fossil fuel combustion, while retene is a peculiar tracer for wood combustion (Goldstein et al., 2008). As for PAHs, their sources include incomplete combustion of coal, fossil fuels or biomass, forest fires, industrial exhaust, traffic release, etc. (Yan et al., 2019; Gao and Ji, 2018). Additionally, $PM_{2.5}$-bound PAHs is a major health concern due to its known carcinogenic and mutagenic properties (Amador-Munoz et al., 2020). Previous studies on PAHs and alkanes are mainly based on traditional off-line method, mainly focusing on seasonal variations of sources and composition characteristics (Feng et al., 2012; Wang et al., 2015; Yang et al., 2021). Only limited studies have characterized the diurnal variations of the components and sources of NPOCs, such as PAHs (Wang et al., 2020), based on online measurement.

The coarse temporal resolution and labor-intensive nature of traditional NPOCs quantification method hugely hinder the utilization of the tracer data (Bourotte et al., 2005; Kavouras et al., 2001; Pehnec et al., 2020; Shimada et al., 2020; Vasilakos et al., 2007; Yang et al., 2010). High temporal resolution measurements of molecular organic tracer compounds in ambient OA can provide insight into the diurnal variation of the contributions of emission sources (such as vehicle exhaust and cooking) and the secondary aerosol formation processes, therefore help formulate effective $PM_{2.5}$ control strategies. Several studies have demonstrated the utility of the high temporal-resolution measurements based on thermal desorption aerosol gas chromatography–mass spectrometry (TAG) (Kreisberg et al., 2009) system. With the ability to obtain hourly data of organic markers, the TAG system can capture the dynamic change of emission sources and atmospheric aging, which can provide observational evidence to support refined source apportionment of $PM_{2.5}$ (Wang et al., 2020; He et al., 2020; Li et al., 2020a, 2020b; Zhao et al., 2013). On the other hand, hourly-resolution TAG data are also useful for pollution episode analysis, as

pollution episodes typically last for a few hours or days and traditional low time-resolution observation are difficult to capture the episodic dynamics.

In this study, a field campaign was conducted for hourly-resolution NPOCs measurement covering the summer and autumn season in Shanghai in order to look into the abundance and temporal variations (especially the diurnal variations) of the $PM_{2.5}$-bound NPOC components. We further focus on episodic analysis, identify the potential source region, quantify the overall contribution of different sources, capture the variation of source contribution and access health impacts of PAHs. This study is necessary and important to guide future organic tracer-based source apportionment analysis and is also of great scientific and practical significance in further reducing $PM_{2.5}$ in Shanghai.

2. Methodology

2.1. Site description and sampling

A field campaign during 1st June to 14th October 2020 was conducted at Shanghai University (SHU, 31.33°N, 121.41°E) in Baoshan district of Shanghai, China. The location and a detailed map with nearby sources are shown in Fig. 1. The sampling site is located in a commercial and residential district, with two arterials roads at ~200 m to the north and ~400 m to the west, respectively. Contemporaneous meteorological data and conventional atmospheric pollutants data ($PM_{2.5}$ and NO_2) were obtained from Shanghai Baoshan Meteorology Station (31.40°N, 121.45°E) (http://data.cma.cn) and Shanghai Hongkou Environmental Monitoring Station (31.30°N, 121.47°E) (http://datacenter.mep.gov.cn), respectively.

The TAG system is placed ~9 m above the ground. NPOC data with a temporal resolution of 2-h was obtained during the observation. The $PM_{2.5}$ sampling started at every even hour of the day at a flow rate about 9 L/min and lasted for 70 min. Field blank samples were collected once every 2 days at a fixed time (2:00–3:00 or 4:00–5:00 a.m.). A total of 418 valid samples and 28 blank samples were collected throughout the campaign, including 286 environmental samples in summer (1st to 5th June, 7th to 12th June, 5th to 9th July, 12th to 18th July, 12th to 18th July, 27th to 31st July, 1st to 8th August) and 132 environmental samples in fall (1st to 14th October), covering approximately 34 diurnal cycles totally.

2.2. Quantification of nonpolar organic compounds in $PM_{2.5}$

The schematic diagram of the TAG deployed in this work is shown in Fig. S1. A detailed description of the working principle of TAG (Aerodyne Research Inc., USA) can be found in previous publications (He et al., 2020; Isaacman et al., 2014; Williams et al., 2006) and is descripted in Text S1. The chemical standards and deuterium-labeled ISs were purchased from o2si (Charleston, South Carolina, USA), ANPEL Laboratory Technologies Inc. (Shanghai, China) and Sigma-Aldrich Chemicals (Bornem, Belgium). We identified the compounds by comparing retention times and mass spectra with those of standards, and then
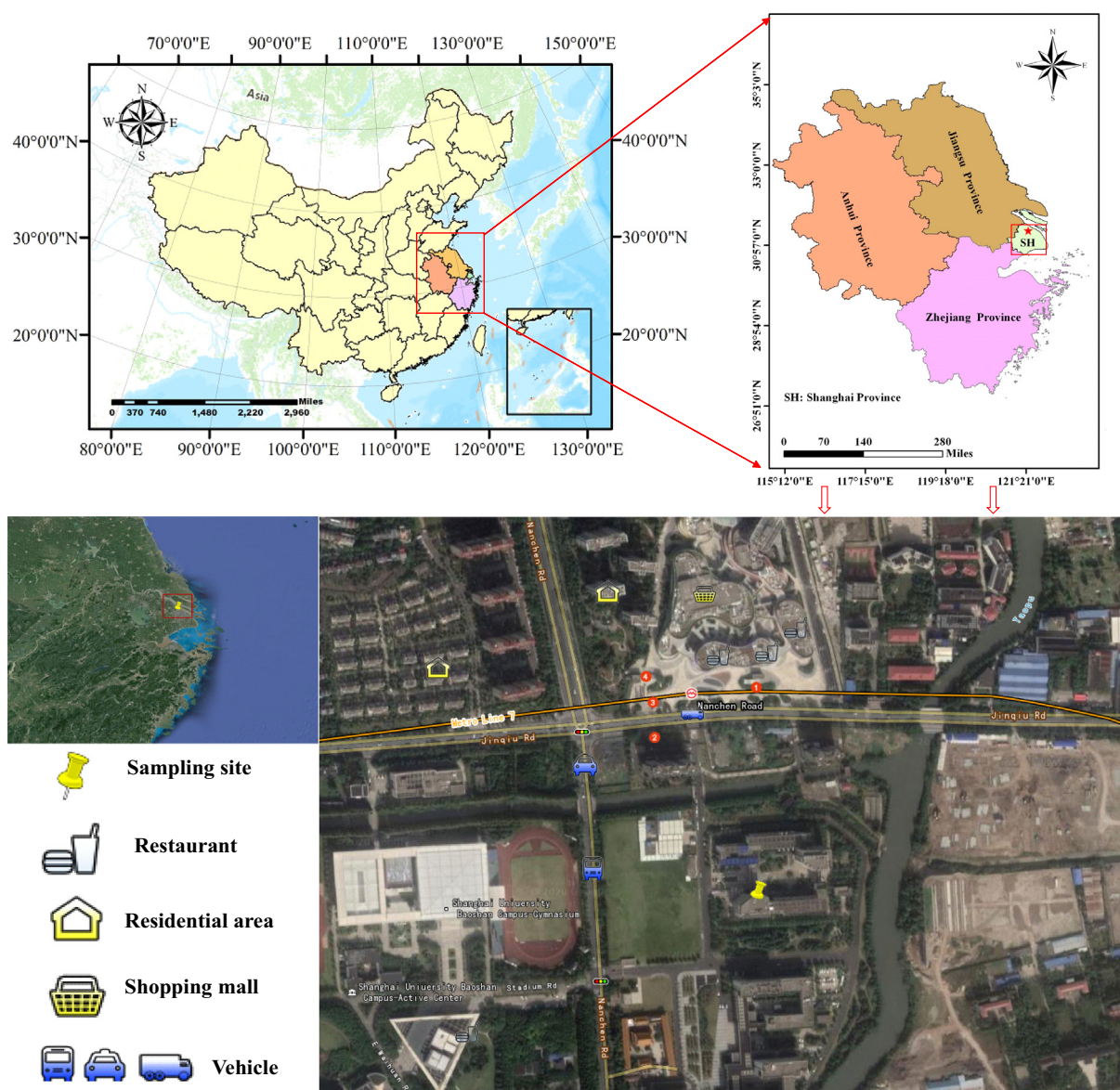
Fig. 1. Location of the sampling site.

quantified by plotting standard curves using the internal standard method. Chromatographic peaks were fitted and integrated using the TERN plug-in program based on Igor v6.37 software, with residuals of peaks less than 10%. During our observation, deuterium-labeled internal standard solution was injected into each sample to monitor instrument condition and analyze contamination levels of species. In this study, we quantified and analyzed a total of 14 PAHs, including Acenaphthylene (Acel), Acenaphthene (Acep), Fluorene (Flue), Phenanthrene (Phe), Anthracene (Ant), Fluoranthene (Flut), Pyrene (Pyr), Benz[*a*]anthracene (BaA), Chrysene (Chr), Benzo[*b*]fluoranthene (BbF), Benzo[*k*]fluoranthene (BkF), Benzo[*a*]pyrene (BaP), Benzo[*ghi*]perylene (BghiP) and Indeno[1,2,3-*cd*]pyrene (IcdP), as well as 15 n-alkanes(C21–C35). Table S1 lists the measured nonpolar organic compounds discussed in this study. The preparation of working external standards and ISs, method detection limits is described in detail in Text S2. Time series of peak areas of ISs are provided in Figs. S4 and S5. The blank samples were collected with the entire sampling flow bypassing the denuder and the CTD and going directly to the pump exhaust, therefore reflecting the residue remaining with the TAG. The blank samples

showed little contamination for the target species in this study (shown in Fig. S3). Due to the negligible signal of quantitative ion of the blank sample, we did not subtract quantitative ion signal of the blank sample from the environmental sample runs. In addition, a standard curve with forced zero-crossing method has been used for the calculation of concentrations.

2.3. Backward trajectory and potential source contribution function (PSCF) analysis

The backward trajectory analysis is a useful tool to investigate the influence of regional transport and local emissions on PM$_{2.5}$ components during the field measurement (Wang et al., 2009). 48-h backward trajectories arriving at an altitude of 500 m above ground level (AGL) over the SHU site were calculated utilizing the 0.2° Global Data Assimilation System (GDAS) meteorological data (https://www.ready.noaa.gov/archives.php). The PSCF values for the grid cells in the study domain are calculated by counting the trajectory segment endpoints that terminate within each cell (Zhang et al., 2020a). The number of

endpoints that fall in the ij^{th} cell is designated n_{ij}. The number of endpoints for the same cell having arrival times at the sampling site corresponding to pollutant concentrations higher than an arbitrarily set criterion is defined as m_{ij}. The PSCF value for the ij^{th} cell is then defined as:

$$PSCFij = \frac{m_{ij}}{n_{ij}} \tag{1}$$

Since the deviation of PSCF results can increase with the distance between cell and receptor, a weight function W_{ij} is introduced to reduce the uncertainty in the PSCF results for grids with fewer air mass trajectories, and the weight function (W_{ij}) is determined according to previous studies (Lyu et al., 2017; Schauer et al., 2002), using the following equation, in which n_{avg} is the average value of the end points per each cell:

$$W_{ij} = \begin{cases} 1.0 & n_{ij} > 3.0 n_{avg} \\ 0.7 & 1.5 n_{avg} < n_{ij} \leq 3.0 n_{avg} \\ 0.4 & 1.0 n_{avg} < n_{ij} \leq 1.5 n_{avg} \\ 0.2 & n_{ij} \leq 1.0 n_{avg} \end{cases} \tag{2}$$

The weighted potential source contribution function (WPSCF) after the introduction of W_{ij} is defined as:

$$WPSCF_{ij} = PSCF_{ij} \times W_{ij} \tag{3}$$

2.4. Diagnostic parameters/ratio

Diagnostic parameters/ratio (DP/R) is a relatively simple but commonly used method to identify sources for certain types of organic molecular compounds in PM$_{2.5}$, such as PAHs and alkanes (Pehnec et al., 2020; Shimada et al., 2020). Diagnostic parameters of n-alkanes, such as carbon maximum number (C_{max}) and carbon preference index (CPI) were adopted for anthropogenic and biogenic source-tracking (Chen et al., 2014; Lyu et al., 2017; Scalan and Smith, 1970; Wang et al., 2019; Xu et al., 2015). C_{max} refers to the carbon number with the highest concentration in the alkane homology. CPI is defined as the concentration ratio of odd-to-even number homologues and is calculated as follows:

$$CPI = \sum_{i=21}^{35} C_i / \sum_{k=22}^{34} C_k \tag{4}$$

where i refers to the odd carbon number, k is the even carbon number from n-alkane series.

As for PAHs, various Diagnostic Ratios (DRs), such as BaP/BghiP, IcP/(IcP + BghiP), BaA/(BaA + Chr), Flt/(Flt + Pyr) and BaP/(BaP + Chr) have been applied to determine their sources (Bourotte et al., 2005; Mehmood et al., 2020; Pehnec et al., 2020). Diagnostic ratios for source identification of PAHs and alkanes used in this study are summarized in SI (Table S3).

2.5. PMF receptor model

The Positive Matrix Factorization (PMF) version 5.0 is applied in this study to conduct source apportionment of non-polar organic components. PMF is a widely used receptor model for source identification of individual types of PM$_{2.5}$-bound organic compounds (such as PAHs) (Cao et al., 2020; Mehmood et al., 2020) and also source apportionment of PM$_{2.5}$ (Li et al., 2020a, 2020b; Ronkko et al., 2020). The rationale is to quantify the contribution of specific sources to the ambient air pollutant concentrations around the receptor site, assuming chemical mass balance between the source and receptor, with the measured concentrations of the species being a linear combination of different sources

(Luo et al., 2019). A detailed description of PMF methods can be found in the SI (Text S5).

2.6. Health risk assessment

We calculated the carcinogenic and mutagenic risk potentials (TEQ and MEQ) of PM$_{2.5}$-bound PAHs by evaluating the Benzo[a]pyrene toxic equivalent concentrations (BaP_{Teq}) and the mutagenic equivalent concentrations (BaP_{Meq}) as indicators of toxicity. The lifetime cancer risk by inhalation (ILCR) of PAHs was also evaluated for four different types of populations (child, adolescent, adult men and adult women). The formulas are as following:

$$TEQ = \sum BaP_{Teq}(PAH) = \sum TEF(PAH) \cdot C(PAH) \tag{5}$$

$$MEQ = \sum BaP_{Meq}(PAH) = \sum MEF(PAH) \cdot C(PAH) \tag{6}$$

$C(PAH)$ represents the concentration of the target PAH, while $TEF(PAH)$ and $MEF(PAH)$ are the toxic equivalency factor and the mutagenic potency factors of the target compound, respectively.

$$ILCR = CSF \times \frac{TEQ \times IR \times EF \times ED}{BW \times AT} \tag{7}$$

Table 1
Statistics of meteorological conditions, hourly concentrations of conventional atmospheric pollutants and TAG measured NPOC species during the campaign.

|	Unit	Mean ± SD	Min.	Max.
Meteorological parameter				
Wind speed (WS)	m/s	2.4 ± 1.5	0.0	8.4
Relative humidity (RH)	%	78.7 ± 15.1	45.0	99.0
Temperature (T)	°C	25.1 ± 4.8	15.2	35.7
Pressure (P)	kPa	100.9 ± 0.7	99.8	102.43
Compounds				
PM$_{2.5}$	μg/m^3	21.6 ± 13.3	1.0	86.0
NO$_2$	μg/m^3	33.5 ± 14	10.0	91.0
TAG measured molecular species				
C21	ng/m^3	0.35 ± 0.14	0.08	1.69
C22	ng/m^3	0.56 ± 0.21	0.11	2.50
C23	ng/m^3	0.68 ± 0.24	0.13	2.35
C24	ng/m^3	0.72 ± 0.26	0.14	3.14
C25	ng/m^3	0.79 ± 0.28	0.20	3.40
C26	ng/m^3	0.78 ± 0.31	0.09	2.63
C27	ng/m^3	0.8 ± 0.37	0.09	4.21
C28	ng/m^3	0.59 ± 0.61	0.04	9.65
C29	ng/m^3	0.84 ± 0.4	0.22	3.37
C30	ng/m^3	0.6 ± 0.32	0.19	2.26
C31	ng/m^3	0.8 ± 0.36	0.14	2.17
C32	ng/m^3	0.46 ± 0.23	0.04	1.65
C33	ng/m^3	0.49 ± 0.32	0.02	2.01
C34	ng/m^3	0.3 ± 0.22	0.01	2.91
C35	ng/m^3	0.25 ± 0.23	0.01	1.53
ΣAlkanes	ng/m^3	8.87 ± 3.46	2.42	27.41
Acel	ng/m^3	0.02 ± 0.02	BMD*	0.48
Acep	ng/m^3	0.04 ± 0.1	BMD*	1.03
Flue	ng/m^3	0.04 ± 0.03	BMD*	1.07
Phe	ng/m^3	0.1 ± 0.04	0.02	1.43
Ant	ng/m^3	0.03 ± 0.06	BMD*	0.56
Flut	ng/m^3	0.07 ± 0.07	BMD*	1.00
Pyr	ng/m^3	0.09 ± 0.07	0.01	1.31
BaA	ng/m^3	0.06 ± 0.07	BMD*	1.87
Chr	ng/m^3	0.09 ± 0.1	BMD*	1.02
BbF	ng/m^3	0.19 ± 0.24	BMD*	1.76
BkF	ng/m^3	0.11 ± 0.19	BMD*	2.27
BaP	ng/m^3	0.08 ± 0.09	BMD*	1.03
BghiP	ng/m^3	0.26 ± 0.23	BMD*	4.31
IcdP	ng/m^3	0.34 ± 0.4	BMD*	2.83
ΣPAHs	ng/m^3	1.27 ± 1.4	0.10	12.68

BMD*: Below method detection limit.
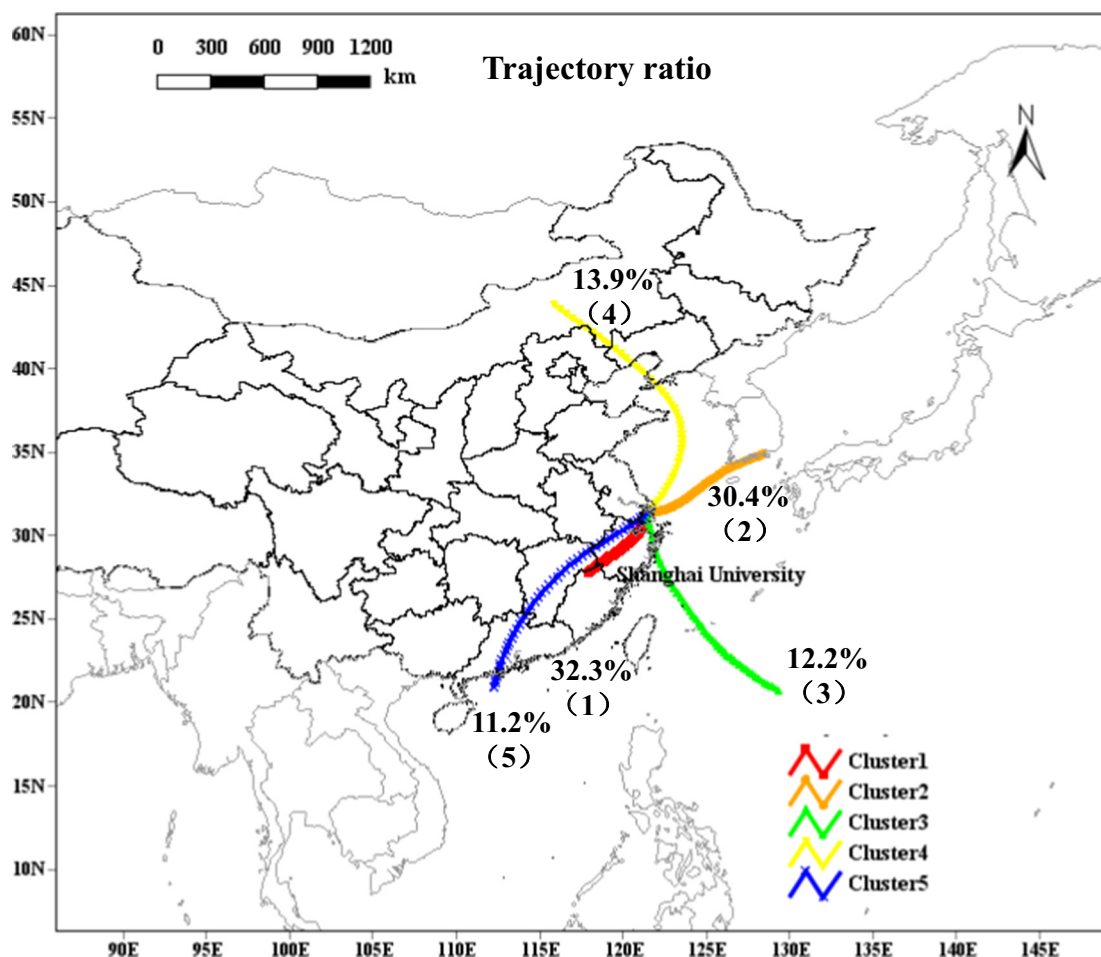
Fig. 2. Distribution of air mass clusters during 1 Jun.–14 Oct., 2020.

Relevant parameters of the three indicators for health risk assessment are further explained in Text S6.

3. Results and discussions

3.1. Overview of the field measurement

Table 1 provides a statistical summary of the concentrations of measured NPOC species, other atmospheric pollutants and meteorological conditions during the campaign. The average temperature (T), relative humidity (RH) and wind speed (WS) was 25.1 ± 4.8 °C, 78.7 ± 15.1% and 2.4 ± 1.5 m/s, respectively. Hourly concentrations of $PM_{2.5}$, alkanes and PAHs ranged from 1 to 86 μg/m^3, 0.1 to 12.68 ng/m^3 and 2.42 to 27.41 ng/m^3, respectively, during the campaign.

Fig. S16 shows box plots of individual concentration for 15 alkanes and 14 PAHs measured during the campaign. It is shown that C27, C29 and C31 dominates the alkanes, while PAHs are dominated by BbF,

BghiP and IcdP, which are consistent with the studies by Feng et al. (2012) and Wang et al. (2015) in previous years.

Depending on the total variation space (TVS) image shown in Fig. S6, the backward trajectories during our observation were classified into 5 air parcel clusters (Fig. 2). Cluster-1, traveling mostly within Zhejiang and Shanghai province, is regarded as local air mass and accounts for 32.3% of the total trajectories. Cluster-2 (30.4%) and cluster-3 (12.2%), coming from the Yellow Sea and the East China Sea, respectively, are regarded as coastal transport air masses. Cluster-4 (13.9%) is the longest, traveling from the inland of northeastern China throughout Yellow Sea and the Bohai Sea region, while cluster-5 (11.2%) was exactly opposite to cluster-4, originating from the inland of southeastern China.

In this study, we defined PAHs over 7 ng/m^3 as PAHs episodes and alkanes above 15 ng/m^3 as alkanes episodes. The 8 episodes was shaded in Fig. 3, with PAHs episodes in gray, alkanes episodes in yellow, and alkanes-PAHs joint episodes in red. The occurrence time of 8 episodes was also list in Table 2. The periods with peak concentrations tend to

Table 2
Statistics of occurrence time of 8 episodes shaded rectangular boxes in Fig. 3.

Episode no.	1	2	3	4	5	6	7	8
Episode type	PAHs	Alkanes	Alkanes	Alkanes-PAHs joint	Alkanes	Alkanes-PAHs joint	Alkanes	Alkanes-PAHs joint
Period	2020-6-10 12:00–14:00	2020-7-5 22:00–2020-7-6 8:00;2020-7-6 20:00–2020-7-7 0:00	2020-7-12 10:00;2020-7-13 0:00–6:00	2020-7-27 20:00–22:00	2020-8-8 8:00–10:00	2020-10-1 18:00,20:00	2020-10-8 12:00	2020-10-9 8:00,14:00;2020-10-10 4:00–10:00;2020-10-11 2:00,6:00,10:00

Table 3

Summary of the seasonal-mean concentrations or concentrations range of PM$_{2.5}$, PAHs, and alkanes derived from previous studies in Shanghai.

District	Sampling year	Sampling season	N of samples	PM (μg/m³)	N of Alkanes	∑Alkanes/(ng/m³)	∑PAHs/(ng/m³)	N of PAHs	Sampling areas	References
Xujiahui	2009	Winter	17	91(PM$_{2.5}$)	21(C16-C36)	90.3	36.6	21	Residential/commercial/traffic	Feng et al., 2012
Yangpu	2011	Fall	20	PM$_{2.5}$	NA	NA	20.5	16	Residential/traffic	Wang et al., 2015
Yangpu	2011	Winter	20	PM$_{2.5}$	NA	NA	27.2	16	Residential/traffic	Wang et al., 2015
Yangpu	2011	Summer	9	PM$_{2.5}$	20(C14-C33)	67.8	8.4	16	Residential/commercial	Wang et al., 2017
Yangpu	2011	Fall	20	80.6(PM$_{2.5}$)	20(C14-C33)	85	NA	NA	Residential/commercial/traffic	Wang et al., 2016a
Yangpu	2011	Winter	18	s104.3(PM$_{2.5}$)	20(C14-C33)	91.4	NA	NA	Residential/commercial/traffic	Wang et al., 2016a
Yangpu	2012	Summer	15	PM$_{2.5}$	NA	NA	6.4	16	Residential/traffic	Wang et al., 2015
Yangpu	2012	Spring	21	PM$_{2.5}$	NA	NA	13.7	16	Residential/traffic	Wang et al., 2015
Yangpu	2012	Summer	40	20-140(PM$_{2.5}$)	14(C5-C18)	40-100	0.12-0.5	16	Residential/traffic	Xu et al., 2015
Yangpu	2012	Spring	19	89.6(PM$_{2.5}$)	20(C14-C33)	181.4	NA	NA	Residential/commercial/traffic	Wang et al., 2016a
Yangpu	2012	Summer	14	57.8(PM$_{2.5}$)	20(C14-C33)	62.5	NA	NA	Residential/commercial/traffic	Wang et al., 2016a
Changning	2013	Winter	11	PM$_{2.1}$	24(C14-C37)	~200	26.2-26.7	12	Industrial/commercial	Wang et al., 2019
Xuhui	2013	Summer	5	PM$_{2.1}$	NA	NA	0.27	9	Residential/traffic	Yang et al., 2021
Xuhui	2013	Winter	6	PM$_{2.1}$	NA	NA	3.03	9	Residential/traffic	Yang et al., 2021
Xuhui	2014	Summer	10	PM$_{2.5}$	19(C18-C36)	52.6	15.3	20	Residential/commercial/traffic	Gao et al., 2018a, 2018b
Qingpu	2014	Summer	10	PM$_{2.5}$	19(C18-C36)	47.9	16.9	20	Farmland/residential	Gao et al., 2018a, 2018b
Lin-Gang Special Area	2014	Summer	10	PM$_{2.5}$	19(C18-C36)	13.3	0.17	20	Coastal	Gao et al., 2018a, 2018b
Minhang	2015	Spring	31	67.83(PM$_{2.5}$)	NA	NA	17.59	16	Urban	Liu et al., 2018
Minhang	2015	Summer	29	56.59(PM$_{2.5}$)	NA	NA	6.81	16	Urban	Liu et al., 2018
Minhang	2015	Fall	32	75.36(PM$_{2.5}$)	NA	NA	46.2	16	Urban	Liu et al., 2018
Minhang	2015	Winter	30	101.07(PM$_{2.5}$)	NA	NA	61.93	16	Urban	Liu et al., 2018
Xuhui	2015	Summer	6	PM$_{2.1}$	NA	NA	0.38	9	Residential/traffic	Yang et al., 2021
Xuhui	2015	Winter	6	PM$_{2.1}$	NA	NA	2.78	9	Residential/traffic	Yang et al., 2021
Xuhui	2017	Summer	7	PM$_{2.1}$	NA	NA	0.42	9	Residential/traffic	Yang et al., 2021
Xuhui	2017	Winter	7	PM$_{2.1}$	NA	NA	2.31	9	Residential/traffic	Yang et al., 2021
Xuhui	2018	Winter	269	47.4(PM$_{2.5}$)	NA	NA	0.31	11	Urban	He et al., 2020
Baoshan	2020	Summer	286	26.3(PM$_{2.5}$)	15(C21-C35)	10.09	0.89	14	Residential/traffic	This study
Baoshan	2020	Fall	132	12.4(PM$_{2.5}$)	15(C21-C35)	6.86	2.08	14	Residential/traffic	This study

coincide with the unfavorable meteorological conditions of low temperatures, high relative humidity and low wind speeds. The causes and major source contributions of these eight episodes is further investigated in Section 3.2 using the diagnostic parameters/ratio, PSCF, and PMF methods. On the contrary, the periods from 1st to 4th August with relative lower and constant NPOC concentrations (dominated by trajectories of cluster3 from the southeastern ocean) are prone to occur with higher temperature, lower relative humidity and higher wind speed. Figs. S14 and S15 show the diurnal variations of average concentration of individual PAH, alkane and NO_2 during the campaign. There is a similar diurnal trend of BbF, BghiP and IcdP, which are high molecular weight PAHs abundant in emissions from vehicles (Kam et al., 2012; Liu et al., 2015). Besides, diurnal trends of BbF, BghiP and IcdP are also similar to NO_2 (Fig. S14), with higher hourly average concentrations during morning hours, which indicated the influence of morning rush hour. With similar diurnal trends, the hourly average concentrations of Flut, Pyr and BaA peaks at 12:00, while Acel and Flue reached the maximum at 14:00. As for alkanes, similarity of diurnal trend appears on C21 and C22. Fossil-fuel-derived n-alkanes are mainly low molecular weight (LMW) alkanes (C18–C25) without odd/even number preference (Li et al., 2013). Since there are few studies on the diurnal variations of individual alkanes in the previous literature, we can only speculate that it may be associated with fossil-fuel consumption activities. Such information should be further investigated with polar organic tracers with stronger source characteristics to provide fine source variation information.

According to the summary results of previous studies listed in Table 3, the seasonal changes of PAH and alkanes showed an overall trend of winter>spring>autumn>summer, and the PAH concentrations changed with $PM_{2.5}$ level. Compared with previous studies, the concentration level of alkane and PAHs in this study is lower among the residential and traffic sampling sites, which may be largely attributed to the air pollution control measures conducted during 2013–2017 and the Blue-Sky Prevention Action during 2018–2020 (http://www.mee.gov.cn), lower traffic and social activities affected by the COVID-19 pandemic (Chu et al., 2021), plus relatively favorable meteorological conditions during summer and fall seasons (Wang et al., 2017). Additionally, the concentration of alkanes and PAHs in this study is most similar to the Lin-Gang Special Area in the summer of 2014 (Gao et al., 2018a, 2018b). We compared historical concentration trend of 14 $PM_{2.5}$-bound PAHs in summer and autumn, respectively, where the data for 2020 was obtained from this study and the data for historical years are from previous literatures. Assuming negligible differences between sampling sites in Shanghai, as shown in Fig. 4, $PM_{2.5}$-bound PAHs concentrations in Shanghai show an overall decreasing long-term trend in summer and fall. This is consistent with the study of Li et al. (2020a, 2020b), which also found a significantly decreasing concentration of BaP since 2001. It is possibly linked to the vigorous emission reduction measures enforced by the government over the past few years (http://www.mee.gov.cn).

3.2. Source identification of nonpolar organic compounds

3.2.1. Potential source contribution function analysis

Fig. 5 shows the PSCF result of $PM_{2.5}$ during the observation period. Higher values of PSCF indicate a higher probability of pollution originating from the region. As shown in Figs. 6–7, the distribution of potential sources of $PM_{2.5}$ and alkanes are similar, both exhibiting hot spots around the middle and lower reaches of the Yangtze River Plain, including Anhui, Jiangxi and Zhejiang provinces, as well as local area. Mainly derived from the transmission of cluster-1 and cluster-5, alkanes and $PM_{2.5}$ pollution is mostly influenced by the superposition of local emissions and emissions from southern provinces. Due to higher temperature and higher vegetation coverage in southeast area in June and July during the sampling period, emissions of plant wax alkanes increased (Wang et al., 2016a). At the same time, the frequent agricultural activities would produce a lot

of soil dust, which is a natural source of PM (Sak et al., 2018). The use of agricultural machinery and local vehicles also increased the emission of alkanes from fossil fuel along with increasing $PM_{2.5}$ emissions (Lyu et al., 2017). Therefore, plant, agriculture and traffic activities jointly contributed to the high concentrations of alkanes and $PM_{2.5}$ in middle and lower reaches of the Yangtze River Plain. However, high PAHs concentrations were tightly associated with air masses from cluster-2 and cluster-4, with an average contribution of 29% and 31%, respectively. High PSCF value region of PAHs concentrated in northeast China, the Yellow Sea and the Bohai Sea, which indicates that PAHs pollution may be more affected by biomass burning during autumn harvest in northern China (Wu et al., 2018) and shipping activities (Su et al., 2020).

In the case of relatively good air quality, traditional filter sampling often takes up to 6–12 h for a single sample, sometimes a full day, which makes it difficult to perform PSCF analysis with the actual corresponding sampling time point trajectory. We averaged the hourly concentration data to obtain the daily mean concentration, and selected the meteorological trajectory at 12:00 a.m. each day to simulate PSCF analysis of traditional filter sampling method. As shown in Fig. S7, the PSCF analysis using daily average concentration can't clearly distinguish the difference between the potential source regions of $PM_{2.5}$-bound PAHs and alkanes, thus also further illustrating the advantage of the high time-resolution data obtained by TAG to finely identify the source regions of pollutants.

3.2.2. Sources analysis of alkanes

Alkanes are common organic compounds in $PM_{2.5}$, which are from both anthropogenic and natural emissions. When CPI is close to 1, n-alkanes are mainly from anthropogenic sources such as fossil fuel combustion and biomass burning (Fang et al., 2015); when $1 < CPI < 3$, n-alkanes are influenced by both biogenic sources (e.g., higher plant activities, bacteria) and anthropogenic sources (e.g., fossil fuels, motor vehicle exhaust) (Yi et al., 2020; Zhao et al., 2007a, 2007b). The observed CPI value during the campaign ranged from 0.3 to 2.0 (Fig. S6), indicating contributions from both biogenic and anthropogenic sources. High C_{max} values elucidate a relatively large contribution from biogenic sources, while low C_{max} values indicate a relatively large contribution from petroleum residues (Gao et al., 2018a, 2018b). Furthermore, high correlation between C21–C25 and C30–C33 shown in Table S8 indicate two common sources for these two groups of alkanes. Zhao et al. (2007a, 2007b) analyzed the chemical composition of particulate organic matter (POM) in $PM_{2.5}$ emitted from western-style fast food and four different Chinese cooking styles, and found the C_{max} of alkanes of catering fumes from western cooking is approximately C25–C26, with a relatively high concentration of C27–C28. Some researches show that C_{max} for petrol vehicles ranges from C18 to C22, while the C_{max} for diesel vehicles is C21 (Ma et al., 2020; Fang et al., 2015). Fig. 5 shows the time series of two indices of alkanes. Throughout the sampling period, C_{max} fluctuates between C22–C33, which demonstrated the combined result of anthropogenic and natural sources for alkanes. However, there is a significant difference of C_{max} between June–August and October. In June–August period, C_{max}

Table 4
Summary of average CPI, C_{max} and dominant cluster during different periods.

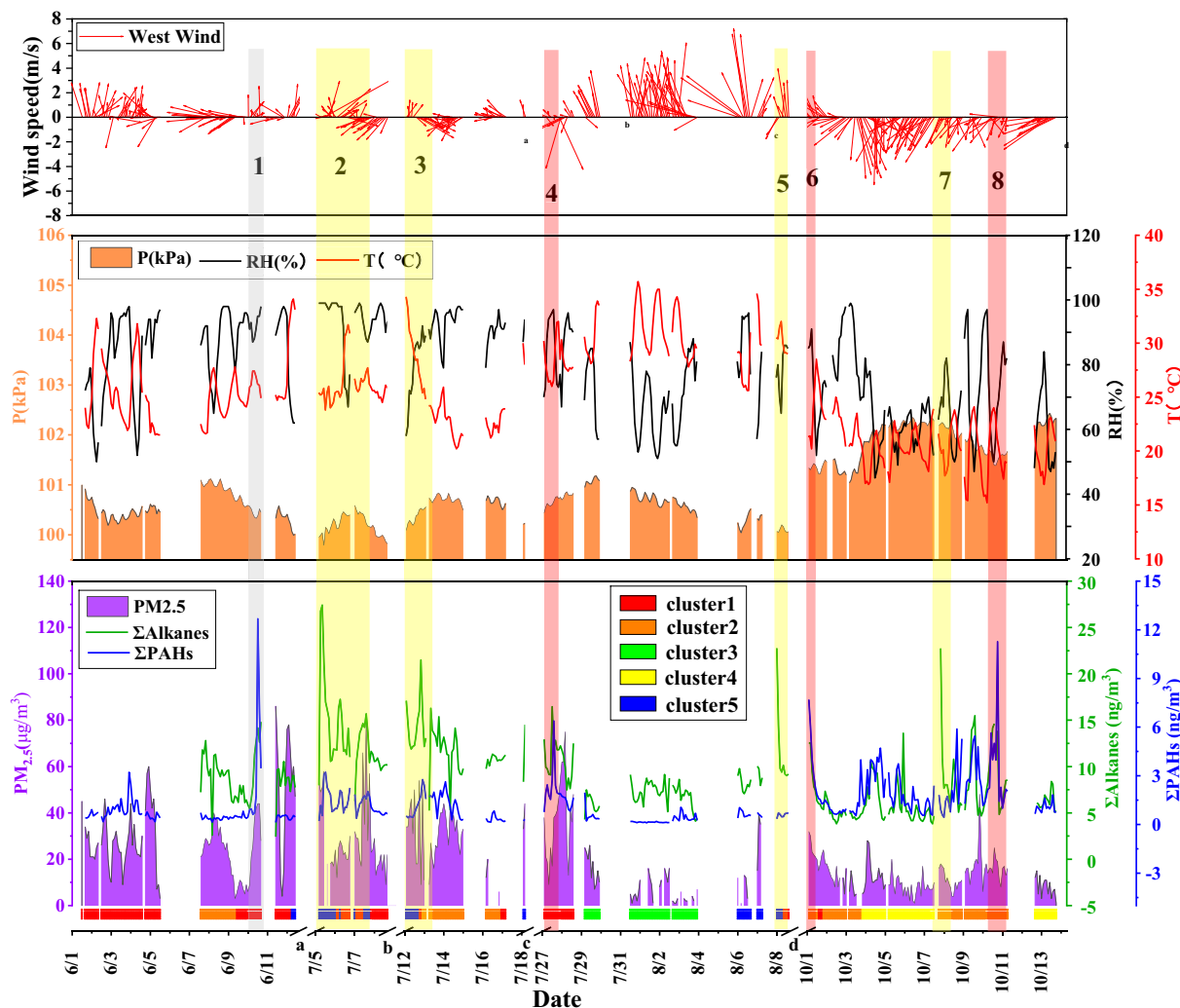| Period	Average CPI	Cmax
June to August	1.24	C22–C25(1.8%), C25–C28(31%), C29–C31(48%), C33–C34 (17.8%)
October	1.25	C22–C25(60.5), C25–C28(11.6), C29–C31(10.8%), C33–C34(17.1%)
Episode2	1.31	C27(66.7%), C29(11.1%), C31(22.2%)
Episode3	1.1	C27(62.5%), C28(12.5%), C29(25.0%)
Episode4	1.4	C31
Episode5	1.1	C27
Episode6	1.3	C27(50%), C31(50%)
Episode7	0.93	C24
Episode8	1.37	C33

Fig. 3. Time series of meteorological parameters, ΣAlkanes, ΣPAHs measured by TAG and PM$_{2.5}$ concentrations, as well as trajectory clusters during the campaign (Missing data of ΣAlkanes during June 1st–5th are caused by lack of corresponding IS quantification).
a, c: Column replacement, b: Instrument Maintenance, d: Repair of mass flow controller of derivatization (MFCDVZ) and column replacement, other short time period gap: Instrument maintenance or quality control tests, such as injecting external standards to check the column efficiency, cleaning ion source and so on.)

concentrated more on C29–C31, accounting for 48.7%, indicating the PM$_{2.5}$-bound alkanes in summer were mainly from biogenic pellet sources. In contrast, in October, C$_{max}$ exhibited a higher proportion on C22–C25 (up to 60.5%), suggesting the predominant contribution from fossil fuel combustion (Table 4). Seven episodes of alkanes (>15 ng/m^3) are also marked with yellow or red light-transparent rectangular boxes

in Fig. 3. Episode 2, 3 and 5 are caused by cooking aerosols, while episode 7 is mainly affected by fossil fuel combustion. Biogenic pellet source has larger contribution to episode 4 and 8. Diurnal variation of C$_{max}$ proportion between June–August and October (Fig. 8) also verified the shift of dominant source of alkanes between summer and fall.
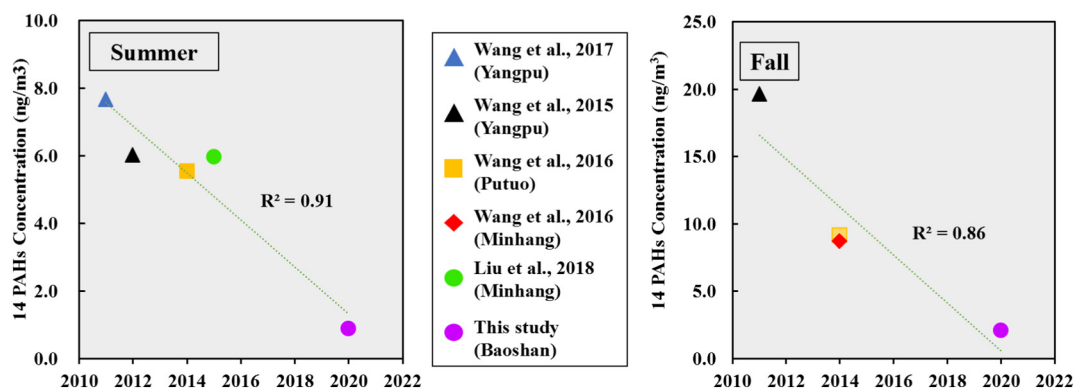
Fig. 4. Long-term trends in 14 PM$_{2.5}$-bound PAHs concentrations of Shanghai in summer and fall.
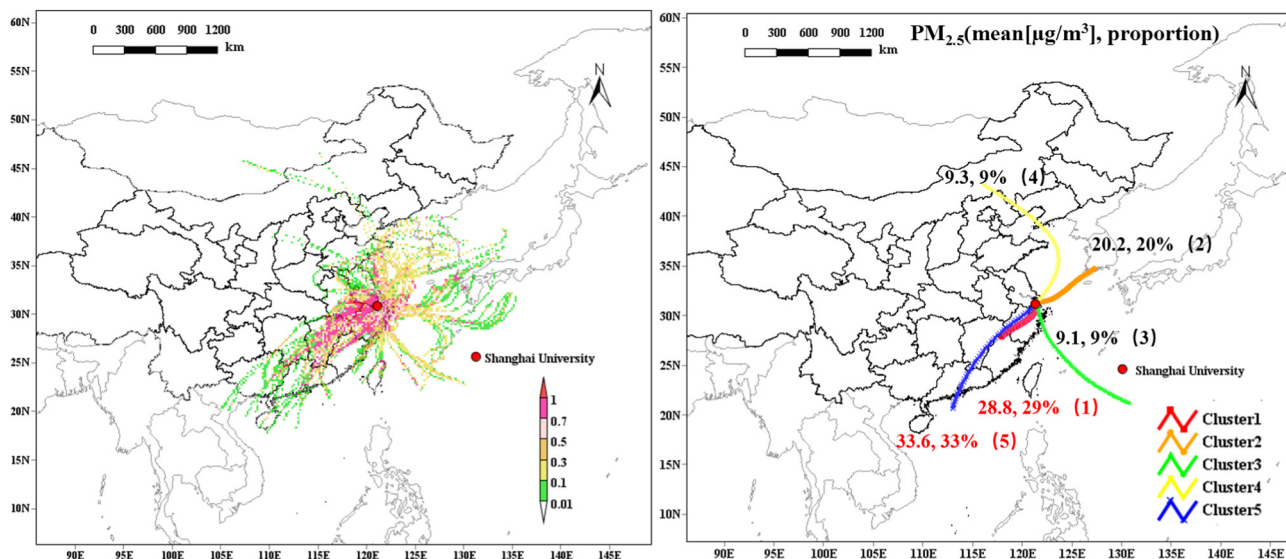
Fig. 5. PSCF analysis (left) and the proportion of mean PM$_{2.5}$ concentrations in each cluster (right) using hourly data during 1 Jun.–14 Oct., 2020.

3.2.3. Source apportionment of PAHs

In this study, we applied various diagnostic ratios such as IcdP/(IcdP + BghiP), BaP/BghiP, Flut/(Flut + Pyr) and BaP/(BaP + Chr) to investigate the potential sources of PAHs during the observation period. According to Biache et al. (2014), Wiriya et al. (2016) and Pehnec et al. (2020), the Flut/(Flut + Pyr) ratio can be used to distinguish vehicle exhausts (0.2–0.4), liquid fossil fuel combustion (0.4–0.5), and grass, wood or coal combustion (>0.5) sources of PAHs, whereas BaP/BghiP ratio can further identify PAHs from different fuel combustion sources, such as gasoline (0.3–0.45), diesel (0.45–0.8) and coal (>0.5) (Pehnec et al., 2020; Romagnoli et al., 2017; Agudelo-Castañeda and Teixeira, 2014). The IcdP/(IcdP + BghiP) ratio values between 0.35 and 0.7 indicate petroleum and diesel sources, while values >0.7 indicate grass, wood or coal combustion sources (Alfonso Murillo-Tovar et al., 2018; Pehnec et al., 2020; Wiriya et al., 2016). Car with catalysts, gasoline combustion, and diesel combustion could be distinguished if BaP/(BaP + Chry) ratio is lower than 0.33, between 0.33 and 0.46, and between 0.46 and 0.7, respectively (Pehnec et al., 2020; Romagnoli et al., 2017; Teixeira et al., 2012). As presented in Fig. 9, the PAHs diagnostic ratios for all samples ranged from 0.2–0.6, 0–2.0, 0–1.1 and 0–1 for Flut/(Flut + Pyr), IcdP/(IcdP + BghiP),

BaP/(BaP + Chry) and BaP/BghiP, respectively. Although the ratio scatter distribution showed a wide range of PAH sources during the sampling period, significantly higher frequency fell on gasoline and diesel. Considering the source distribution shown in Fig. 1 and PSCF analysis, it is reasonable to deduce that local gasoline and diesel vehicles emissions, with diesel vessels emission transported from northeast China and fishing grounds in the Yellow and the Bohai Seas, were the primary PM$_{2.5}$-bound PAHs sources at the sampling site.

PM$_{2.5}$-bound PAHs are relatively stable and can be transported over long distances (ChooChuay et al., 2020; Yan et al., 2015); therefore, they are suitable as tracers of source apportionment. 2–9 factors were tested to determine the optimal factor number by examining the changes in $Q_{(true)}/Q_{(exp)}$ (Fig. S9), and factors were finally distinguished for further PMF analysis. In PMF, the optimal number of factors is a compromise between identifying factors with the best physical explanations and achieving a sufficiently good fit for all species. The change of Q(true)/Q(exp) values is often used as a reference for the determination of factor number. Although Q(true)/Q(exp) can gradually decrease as the number of factors keeps increasing, the optimal number of factors tends to occur when the Q(true)/Q(exp) changes less dramatically. As shown in Fig. S9, Q(true)/Q
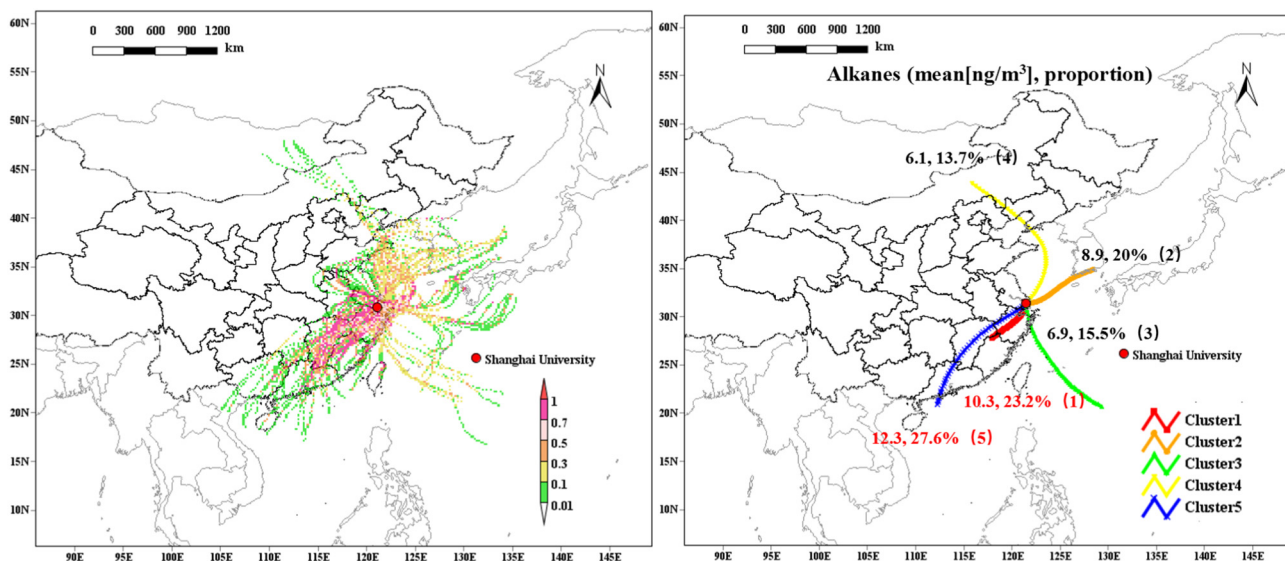

Fig. 6. PSCF analysis (left) and the proportion of mean PM$_{2.5}$-bound Alkane concentrations in each cluster (right) during 1 Jun.–14 Oct., 2020.
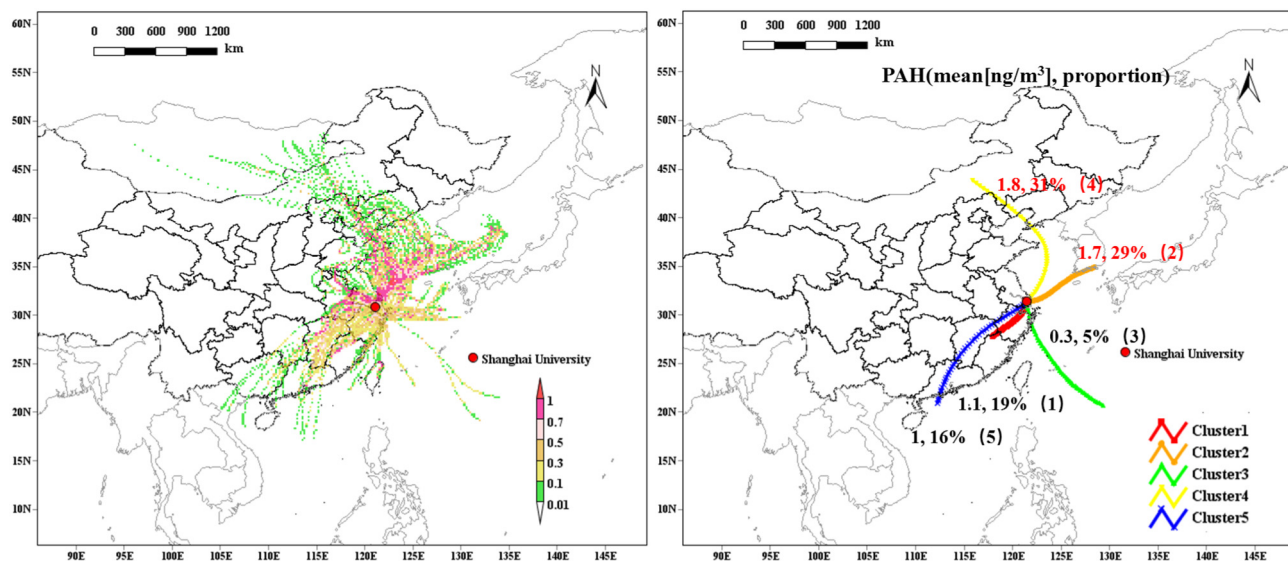
Fig. 7. PSCF analysis (left) and the proportion of mean PM$_{2.5}$-bound PAHs concentrations in each cluster (right) during 1 Jun.–14 Oct., 2020.

(exp) decreased by 12.3%–14.1% from 4-factor to 9-factor runs, less significant than the 15.6–21.1% reduction from 2-factor to 4-factor runs, suggesting that 4-factor run should be optimal solution. The BS factors from the resampled data matrices are mapped to the base run factors to provide the reproducibility of different base run factors due to the random errors. It is suggested that factor mapping higher than 80% indicates robust factors. DISP mainly explores rotational ambiguity in the PMF results. In DISP, the first value is an error code: 0 means no error; 6 or 9 indicates that the run was aborted. If this first value is non-zero, the DISP analysis results are considered invalid. Generally, BS and DISP results shown in Table S4 indicated robust factor solutions. In addition, when examining the factor profiles, the 4-factors solution also provides the most reasonable source profiles. Source profiles of the 4 factors resolved in the PMF model are presented in Fig. 10, in which the column corresponds to the PAHs contribution profiles and the black dot represents the concentration profile.

Factor 1 was dominated by BaA, BghiP and IcdP, moderately weighted by BbF, and BaP, indicating gasoline sources. Mehmood et al. (2020) and Ravindra et al. (2006) had ascribed source factor with

higher levels of the five and six rings PAHs (BaP, BbF, BghiP and IcdP) to gasoline-powered vehicles. Some tunnel experimental studies had also shown that higher molecular weight PAHs are more abundant in emissions from gasoline engines or light vehicles (Kam et al., 2012; Liu et al., 2015). Meanwhile, high relevance (r ≥ 0.8) between BbF, BaP, BghiP and IcdP shown in Table S9 suggests the same source origin of these PAHs. In addition, profile of factor 1 is similar to the gasoline engine emission factor resolved in PMF study of PAHs in Shanghai by Wang et al. (2015). As shown in Fig. S10, Factor1 had evident variation during the whole campaign, and larger contribution when local air mass cluster 1 dominates, along with higher mean concentration in the morning, noon and afternoon traffic peak hours (Fig. 11). This conclusion is consistent with the 3D-location map in Fig. 1. Two traffic arteries in its vicinity make it reasonable to be classified as a gasoline source.

Factor 2 is characterized by high loadings of BbF and Chr, followed by Pyr, Flut and Phe. This represents coal or catering source of PAHs. The study of Zhao et al. (2019) showed that Nap, Pyr, Chr, and Phe are the main PAHs released from residential cooking. Moreover, the profile of coal combustion is highly loaded with BbF, Chr, Pyr and Flut (Li et al.,
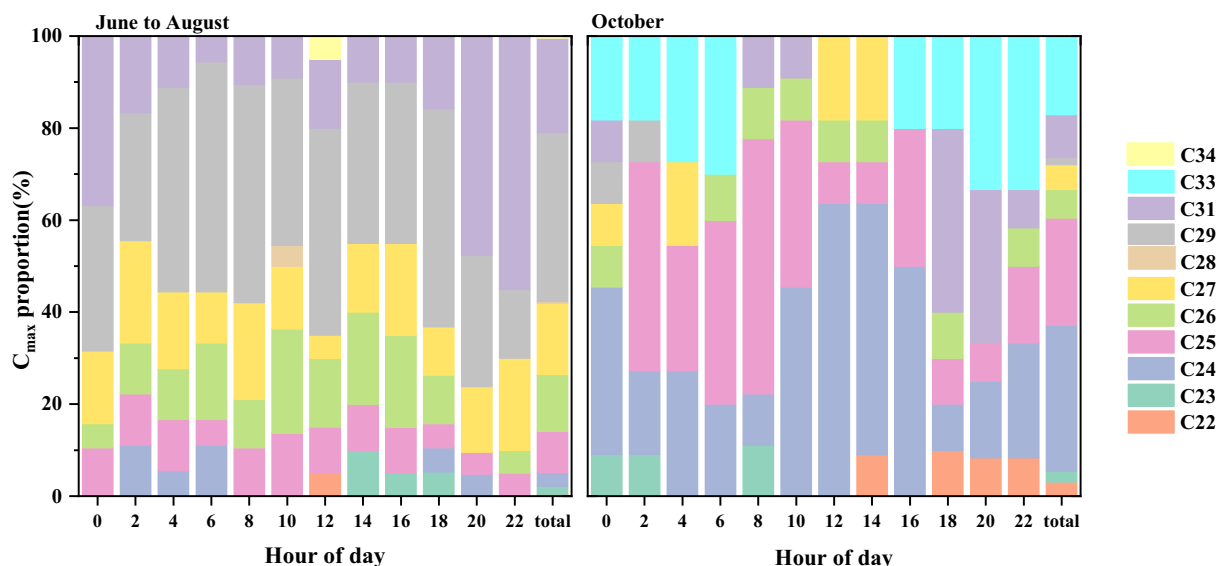

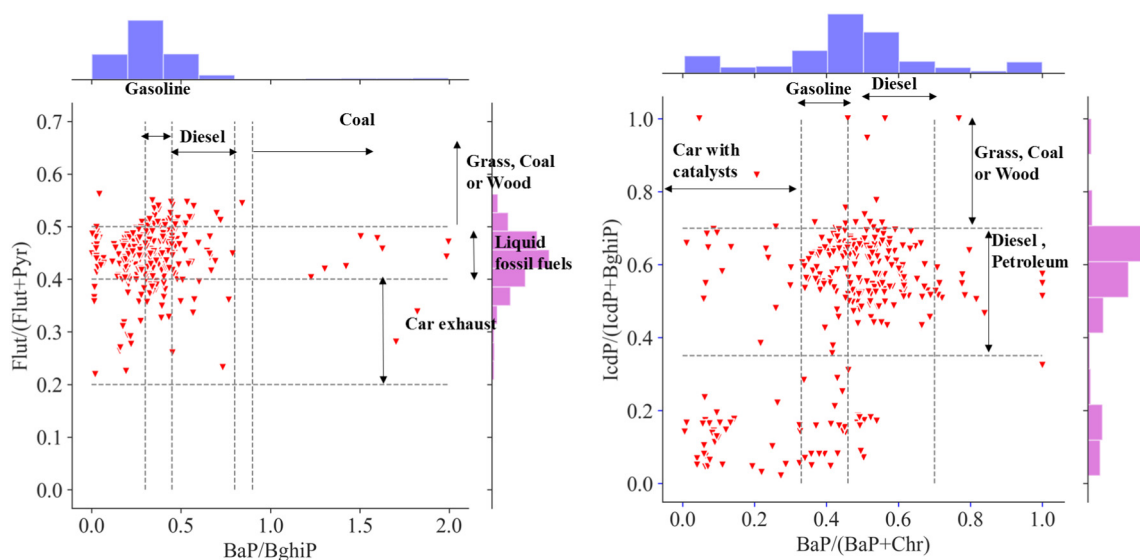**Fig. 8.** Diurnal variation of C$_{max}$ proportion during 1 Jun.–14 Oct., 2020.

Fig. 9. Bivariate and frequency distribution plots for the ratios of (a) Flut/(Flut + Pyr) vs. BaP/BghiP, (b) IcdP/(IcdP + BghiP) vs. BaP/(BaP + Chr) in PM$_{2.5}$ during 1 Jun.–14 Oct.
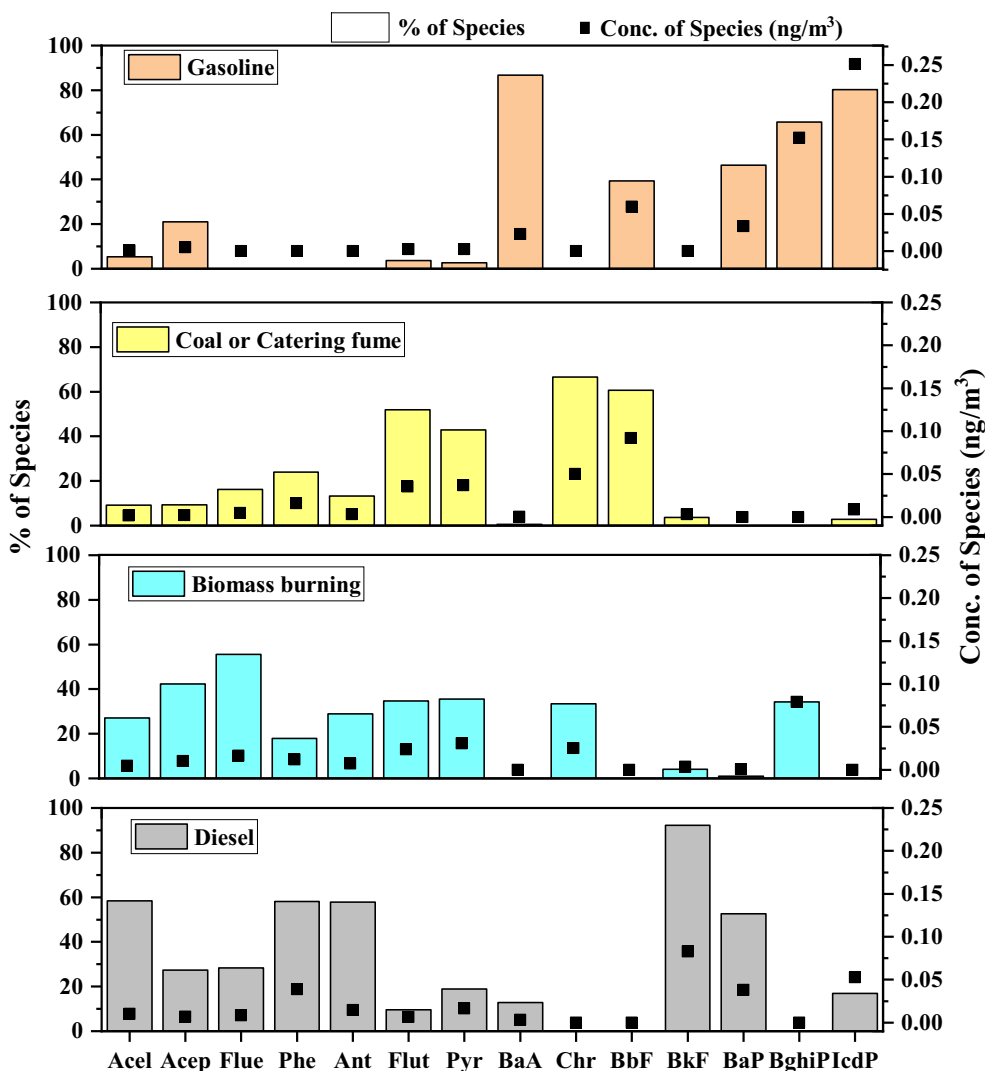

Fig. 10. Source profiles of the 4 factors resolved in the PMF.
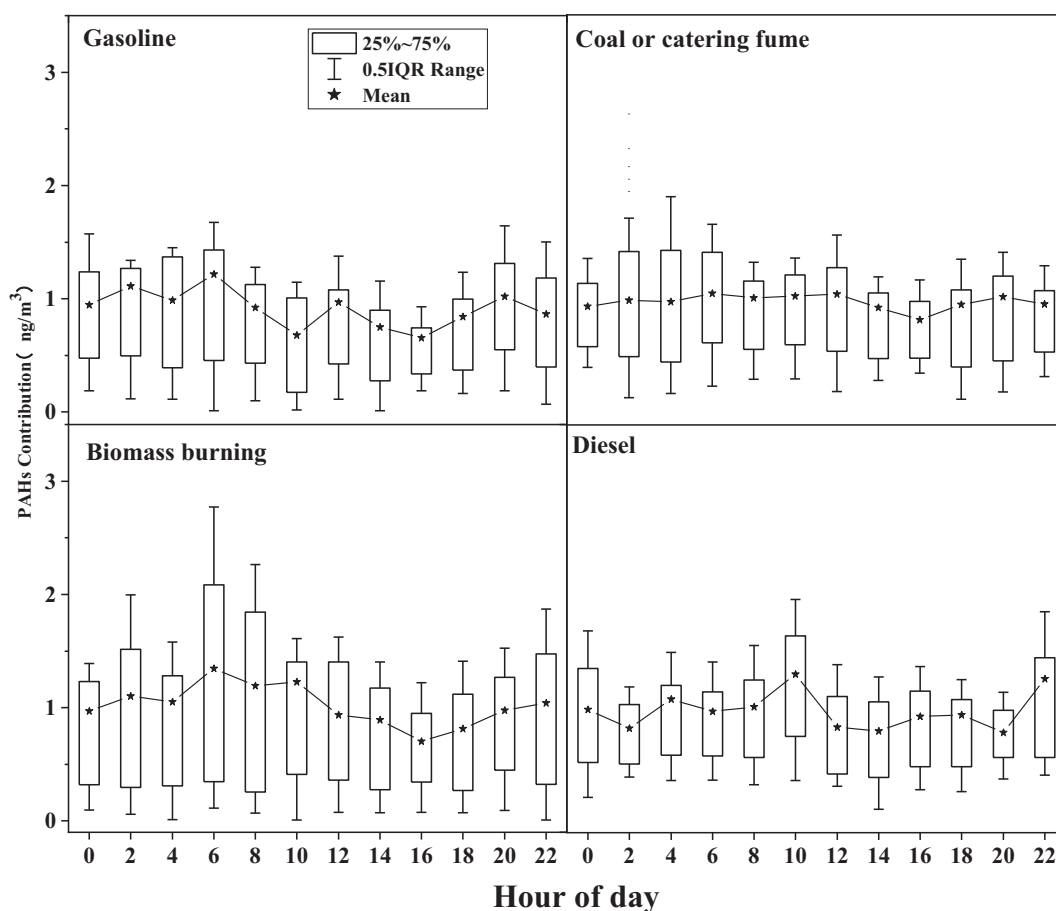
Fig. 11. Diurnal variation of individual source factor resolved by PMF.

2019b; Lin et al., 2015; Ma et al., 2020). Typically, coal combustion and catering fumes could occur simultaneously, such as barbecue stalls using coal as fuel. High correlation (r ≥ 0.8) between Flut, Pyr, BaA, Chr and BbF was found (Table S9). Thus, Factor 2 is considered as coal or catering source. Time series of coal or catering (Fig. S10) showed relatively large variations when dominated by local air mass cluster 1, which indicates the influence of local catering. Notably, diurnal variation in Fig. 11 showed higher concentration during lunch preparation and meal times at 10:00 and 12:00. In October, contribution of Factor 2 became higher and relatively stable when the site was mainly affected by the northern air mass cluster 2 and 4. Li et al. (2019a) analyzed the

seasonal contributions of different sources to NPAHs and OPAHs in PM$_{2.5}$ in North China, and found that coal combustion had higher contribution in fall than summer. With the gradual decrease of temperature, the contribution of coal combustion is greater in October than in summer (Li et al., 2019a; Zhang et al., 2020b), which also led to higher mean concentrations at 20:00 and 22:00.

Factor 3, dominated by Acel, Acep and Flue, moderately weighted by Ant, Pyr, and Flut, is close to biomass burning or straw burning (Li et al., 2019b; Lin et al., 2015; Ma et al., 2020). Experimental studies of source spectra by Leavey et al. (2017) revealed that PAHs from biomass burning is dominated by 2–4 rings, with lower contribution of 5–6 ring
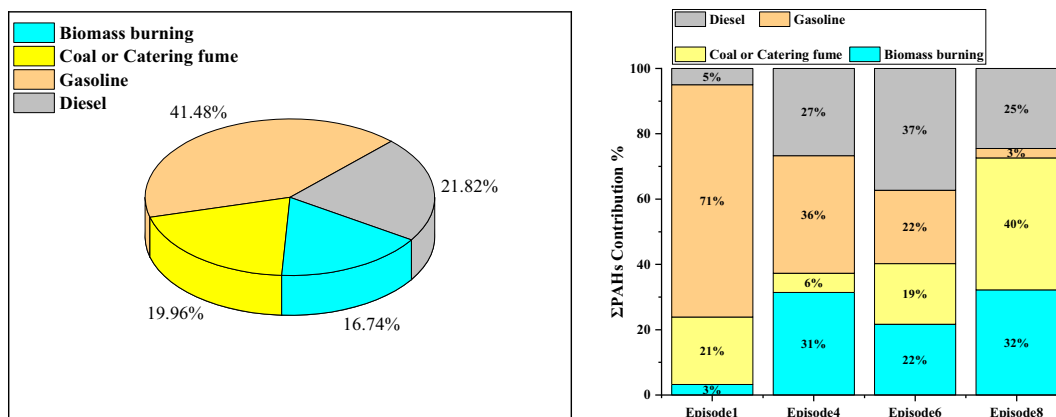

Fig. 12. Percentage contributions of individual source factor to PM$_{2.5}$-bound PAHs during total campaign (left) and 4 episodes (right) based on PMF results.

PAHs. Using the PMF model, source apportionment of $PM_{2.5}$-bound PAHs in Shanghai (Ma et al., 2020) and Harbin (Wang et al., 2015), both showed high loadings of Acel, Acep and Flue in biomass burning factor, which is highly consistent with the result in this study. Furthermore, high correlation (r ≥ 0.9) can be found between Acel and Flue, as well as Flut and Pyr (Table S9). As illustrated in Fig. S10, biomass burning had a significant contribution from July to August in the southern region and in October in the northern area (Huang et al., 2012; Wu et al., 2018). Diurnal variation in Fig. 11 displayed high concentration at early morning and late night. Cheng (2017) had detected higher biomass burning fire points at early morning and night using MODIS contextual algorithm based on VIIRS 375 m data, while the study of Li et al. (2020a, 2020b) showed diurnal variation of biomass burning factor also exhibited higher concentration at early morning and night. This phenomenon may be related to farming practices and the policy of prohibiting straw burning.

Higher loadings of BkF and BaP and moderate loading of 2–3 rings PAHs (e.g., Acel, Phe and Ant) found in Factor 4 indicates diesel combustion such as diesel trucks, crop harvesters, shipping vessels, etc. Wang et al. (2015) identified the factor with high loadings of BkF and BaP, moderately loaded by Phe and Ant as diesel engine emission source, while Liu et al. (2019) reported diesel emissions enriched in Phe and BkF. More affected by the local air mass and diesel truck (Wang et al., 2015) in June, diesel source changed sharply and showed prominent mean concentration at 22:00, which is affiliated with the policy of restricting the passage of diesel trucks during the day. Dominated by cluster-2 and cluster-4, shipping activities (Su et al., 2020) and crop harvesting (Huang et al., 2012; Wu et al., 2018) using diesel fuel in August to October, led to the increasing contribution of diesel source (Fig. S10).

In this study, The PMF model was applied to quantify the contributions of some major source factors to the overall observation process, and examine the contribution changes of various sources for several episodes. Gasoline and diesel emission was the two main sources of PAHs, accounting for 41.48% and 21.82%, respectively (Fig. 12). This is consistent with the results of diagnostic ratios of PAHs (Fig. 9). Coal or catering fume accounts for 30.5% of the measured PAHs, while biomass burning contribution was 16.74%. For Episode 1, due to the influence of cluster 1, the contribution of gasoline vehicle exhaust was prominent, reaching 71%. Although the gasoline source also played a leading role in Episode 2 (36%), its contribution is not as high as in Episode 1. Another source comparable to gasoline source in Episode 2 was biomass burning (31%) in July and is closely linked to summer harvest in southern region. However, the leading sources for Episode 4 and Episode 7 are diesel (37%) and coal or catering (40%), respectively, which is dominated by

cluster 2 and cluster 4, and is highly associated with maritime shipping in the Yellow and Bohai seas and coal consumption in the northern region. Although only 5-months data were obtained in this study, the data (sample size up to 480) is sufficient to explain the source of NPOCs over summer and autumn in Shanghai when compared to the number of samples of other literatures using in PMF model on the same time scale (i.e., the sampling period is the same as summer and autumn), as shown in Table S5.

3.3. Health risk assessment

Fig. S13 shows the time series of three indicators (i.e. TEQ, MEQ and ILCR) of human health risk of 14 PAHs measured over the sampling period. Overall, MEQ is higher than TEQ during the observation period. As opposed to adolescents and children, adults have the higher ILCR by inhalation of $PM_{2.5}$-bound PAH. The value of TEQ ranged from 1.04×10^{-4} to 1.28 ng/m^3, with an average of 0.13 ± 0.16 ng/m^3; while the value of MEQ ranged from 1.85×10^{-3} to 2.44 ng/m^3, with an average of 0.27 ± 0.3 ng/m^3. Most of TEQ and MEQ were lower than the value of 1 ng/m^3 recommended by the European Union (European Commission, 2001) except for several episodes, which means that people are at low mutagenic and toxic potency exposed to $PM_{2.5}$-bound PAH levels during sampling period. The ILCR for the four populations (children, adolescents, adult men and adult women) were 1.30×10^{-8}–1.59×10^{-4} (mean: 1.65×10^{-5}), 1.07×10^{-8}–1.32×10^{-4} (mean: 1.37×10^{-5}), 7.49×10^{-8}–9.20×10^{-4} (mean: 9.53×10^{-5}) and 7.53×10^{-8}–9.25×10^{-4} (mean: 9.58×10^{-5}) during the campaign, respectively. Obviously, the average TEQ, MEQ and ILCR is higher in the fall (TEQ:0.23 ng/m^3; MEQ: 0.44 ng/m^3; ILCR for children, adolescents, adult men and adult women: 2.83×10^{-5}, 2.35×10^{-5}, 1.64×10^{-4} and 1.64×10^{-4}) than in the summer (TEQ:0.09 ng/m^3; MEQ: 0.19 ng/m^3; ILCR for children, adolescents, adult men and adult women: 1.1×10^{-5}, 9.13×10^{-6}, 6.37×10^{-5} and 6.41×10^{-5}) during the campaign.

The diurnal variation of the TEQ, MEQ, ILCRs are shown in Figs. S11–12. Notably, the morning hours (8:00–10:00) and nighttime (20:00–22:00) exhibit higher TEQ, MEQ and ILCR than other time periods. Benzo[a]pyrene toxic equivalent concentrations (BaP_{Teq}) and the mutagenic equivalent concentrations (BaP_{Meq}) of individual PAH show that, BaP had the highest toxic potency while IcdP had the highest mutagenic potency during the campaign. Although BbF, BkF and IcdP only have lower toxic equivalency factors (TEFs) of 0.1 than BaP, they also had high toxic potency due to their high concentrations during the campaign (Fig. 13). On the other hand, IcdP, BbF, BaP and BghiP had high mutagenic potency. Since motor vehicles emit more of these PAHs (Kam et al., 2012; Liu et al., 2019; Liu et al., 2015), control of vehicle sources is
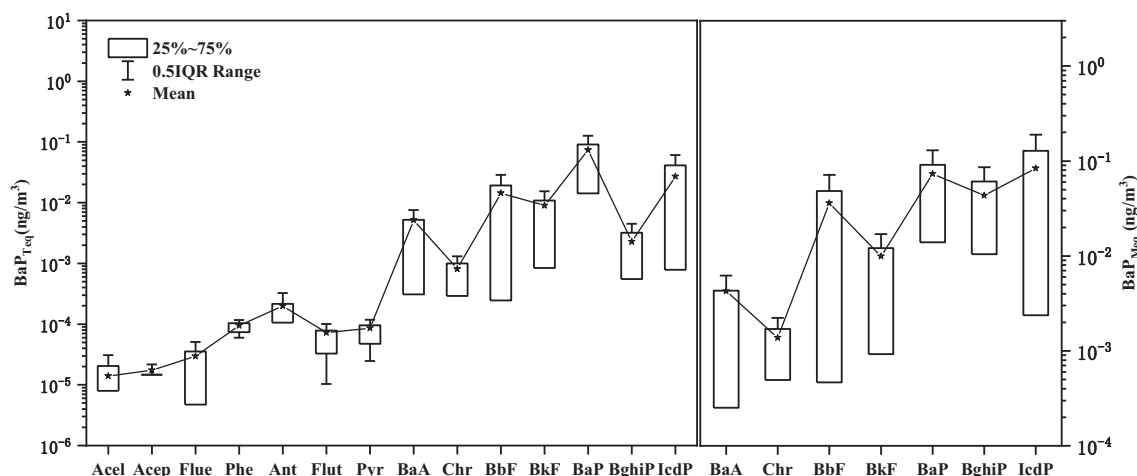

Fig. 13. Benzo[a]pyrene toxic equivalent concentrations (BaP_{Teq}) and the mutagenic equivalent concentrations (BaP_{Meq}) of individual PAH during the campaign.

more effective to reduce its harm for human health. Lack of gaseous PAHs data may lead to bias of health risk assessment of total PAHs. However, due to observational limitation of the instrument, we only obtained PM$_{2.5}$-bound PAHs data during the observation period. In the future study, simultaneously measurement of the concentrations of gaseous and PM$_{2.5}$-bound PAHs is recommended to make up for this gap.

4. Conclusions

In this study, PM$_{2.5}$-bound nonpolar organic compounds including PAHs and alkanes were measured using the online TAG system at every other hour in a seven-week field campaign in urban Shanghai. The average concentration of 14 PAHs and 15 alkanes was 1.27 ± 1.4 ng/m^3 and 8.87 ± 3.46 ng/m^3 during the observation period, respectively. The dominant PAHs species were BbF, BghiP and IcdP, whereas C27, C29 and C31 dominated the alkanes. Time series of CPI and C$_{max}$ of alkanes indicates that alkanes came from a combination of both anthropogenic and biogenic sources during the observation period. Natural sources contribute more to alkanes in summer, while anthropogenic sources contribute more to alkanes in the fall season. Based on backward trajectory clustering and PSCF, the main potential source regions of PM$_{2.5}$ and alkanes were mainly influenced by the air masses of cluster-1 and cluster-5, including middle and lower reaches of the Yangtze River Plain comprising Anhui, Jiangxi and Zhejiang provinces as well as the local areas southwards. On the contrary, the potential source area of PAHs originates from northeastern China. The diagnostic ratio of PAH revealed the significance of gasoline and diesel emission source. Four main sources (gasoline, diesel, biomass burning and coal or catering fume) of PAHs were identified by PMF model at the observation site. Gasoline and diesel emissions were the two major sources during the campaign (41.48% and 21.82%, respectively), followed by coal or catering fume (19.96%) and biomass burning emission (16.74%). Diurnal variation of gasoline source resolved by PMF showed higher concentrations during traffic rush hours, while coal consumption or catering presented higher concentrations during lunch times from 10:00 to 12:00, which is consistent with the corresponding anthropogenic activity time. In addition, the TAG data in conjunction with PMF also can be able to source appointment of short-duration episodes. Human health risk of PAHs indicates that people are at low mutagenic and toxic potency exposed to PM$_{2.5}$-bound PAH levels during sampling period. Adult women are at greater lifetime cancer risk by inhalation (ILCR) of PM$_{2.5}$-bond PAHs than other age groups, and people may be exposed to higher health risks in the morning and evening during the campaign.

CRediT authorship contribution statement

Kun Zhang: Methodology, Investigation, Formal analysis, Writing – original draft. **Liumei Yang:** Methodology, Investigation, Formal analysis, Writing – original draft. **Qing Li:** Methodology, Investigation, Formal analysis. **Rui Li:** Methodology, Investigation, Formal analysis. **Dongping Zhang:** Validation. **Wen Xu:** Validation. **Jialiang Feng:** Validation. **Qiongqiong Wang:** Validation. **Wu Wang:** Validation. **Ling Huang:** Writing – review & editing. **Elly Arukulem Yaluk:** Writing – review & editing. **Yangjun Wang:** Writing – review & editing. **Jian Zhen Yu:** Methodology, Validation, Writing – review & editing. **Li Li:** Conceptualization, Methodology, Writing -review and editing, Funding acquisition.

Declaration of competing interest

The authors declare that they have no conflict of interest.

Acknowledgement

Appendix A. Supplementary data

Supplementary data to this article can be found online at https://doi.org/10.1016/j.scitotenv.2021.148070.

References

Agudelo-Castañeda, D.M., Teixeira, E.C., 2014. Seasonal changes, identification and source apportionment of PAH in PM 1.0. Atmos. Environ. 96, 186–200. https://doi.org/10.1016/j.atmosenv.2014.07.030.

Alfonso Murillo-Tovar, M., Barradas-Gimate, A., Ivonne Arias-Montoya, M., Albeiro Saldarriaga-Norena, H., 2018. Polycyclic aromatic hydrocarbons (PAHs) associated with PM2.5 in Guadalajara, Mexico: environmental levels, health risks and possible sources. Environments. 5. https://doi.org/10.3390/environments5050062.

Amador-Munoz, O., Martinez-Dominguez, Y.M., Gomez-Arroyo, S., Peralta, O., 2020. Current situation of polycyclic aromatic hydrocarbons (PAH) in PM2.5 in a receptor site in Mexico City and estimation of carcinogenic PAH by combining non-real-time and real-time measurement techniques. Sci. Total Environ. 703. https://doi.org/10.1016/j.scitotenv.2019.134526.

Andreae, M.O., Rosenfeld, D., 2008. Aerosol–cloud–precipitation interactions. Part 1. The nature and sources of cloud-active aerosols. Earth Sci. Rev. 89, 13–41. https://doi.org/10.1016/j.earscirev.2008.03.001.

Biache, C., Mansuy-Huault, L., Faure, P., 2014. Impact of oxidation and biodegradation on the most commonly used polycyclic aromatic hydrocarbon (PAH) diagnostic ratios: implications for the source identifications. J. Hazard. Mater. 267, 31–39. https://doi.org/10.1016/j.jhazmat.2013.12.036.

Bourotte, C., Forti, M.C., Taniguchi, S., Bicego, M.C., Lotufo, P.A., 2005. A wintertime study of PAHs in fine and coarse aerosols in Sao Paulo city, Brazil. Atmos. Environ. 39, 3799–3811. https://doi.org/10.1016/j.atmosenv.2005.02.054.

Cao, Z., Wang, M., Shi, S., Zhao, Y., Chen, X., Li, C., et al., 2020. Size-distribution-based assessment of human inhalation and dermal exposure to airborne parent, oxygenated and chlorinated PAHs during a regional heavy haze episode. Environ. Pollut. 263. https://doi.org/10.1016/j.envpol.2020.114661.

Chen, Y., Cao, J., Zhao, J., Xu, H., Arimoto, R., Wang, G., et al., 2014. n-Alkanes and polycyclic aromatic hydrocarbons in total suspended particulates from the southeastern Tibetan Plateau: concentrations, seasonal variations, and sources. Sci. Total Environ. 470, 9–18. https://doi.org/10.1016/j.scitotenv.2013.09.033.

Cheng, L.X., 2017. A Method of Active Fire Detection Based on VIIRS 375m Data and Effects on the Haze Pollution From Autumn Crop Residue Burning Over the Jing-Jin-Ji Region (Master Thesis. (in Chinese)).

ChooChuay, C., Pongpiachan, S., Tipmanee, D., Deelaman, W., Suttinun, O., Wang, Q., et al., 2020. Long-range transboundary atmospheric transport of polycyclic aromatic hydrocarbons, carbonaceous compositions, and water-soluble ionic species in southern Thailand. Aerosol Air Qual. Res. 20, 1591–1606. https://doi.org/10.4209/aaqr.2020.03.0120.

Chu, B., Zhang, S., Liu, J., Ma, Q., He, H., 2021. Significant concurrent decrease in PM2.5 and NO2 concentrations in China during COVID-19 epidemic. J. Environ. Sci. 99, 346–353. https://doi.org/10.1016/j.jes.2020.06.031.

European Commission, 2001. Opinion of the SCF on the risks to human health of Polycyclic Aromatic Hydrocarbons in food. Scientific Committee on Food. http://europa.eu.int/comm/food/fs/sc/scf/index_en.html.

Fang, D.Q., Cai, T.Q., Zhang, Y., Zhang, Y.X., Zhang, Y.H., 2015. Characters of airborne particular matter from vehicular exhausts and oil-powered boiler emissions. Chem. Ind. Eng. 32, 44–51 (in Chinese). 10.13353/j.issn.1004.9533.2015.05.005.

Feng, J., Sun, P., Hu, X., Zhao, W., Wu, M., Fu, J., 2012. The chemical composition and sources of PM2.5 during the 2009 Chinese New Year's holiday in Shanghai. Atmos. Res. 118, 435–444. https://doi.org/10.1016/j.atmosres.2012.08.012.

Gao, Y., Ji, H., 2018. Characteristics of polycyclic aromatic hydrocarbons components in fine particle during heavy polluting phase of each season in urban Beijing. Chemosphere. 212, 346–357. https://doi.org/10.1016/j.chemosphere.2018.08.079.

Gao, Y.-Q., Wang, H.-L., Jing, S.-A., Qiao, L.-P., Li, L., Zhu, S.-H., et al., 2018a. Chemical characterization, spatial distribution, and source identification of organic matter in PM2.5 in summertime Shanghai, China. Huan Jing Ke Xue 39, 1978–1986. https://doi.org/10.13227/j.hjkx.201708197.

Gao, Y-q., Wang, H-l., Jing, S-a., Qiao, L-p., Li, L., Zhu, S-h., et al., 2018b. Chemical characterization, spatial distribution, and source identification of organic matter in PM2.5 in summertime Shanghai, China. Environ. Sci. 39, 1978–1986 (in Chinese). 10.13227/j.hjkx.201708197.

Goldstein, A.H., Worton, D.R., Williams, B.J., Hering, S.V., Kreisberg, N.M., Panic, O., et al., 2008. Thermal desorption comprehensive two-dimensional gas chromatography for in-situ measurements of organic aerosols. J. Chromatogr. A 1186, 340–347. https://doi.org/10.1016/j.chroma.2007.09.094.

He, X., Wang, Q., Huang, X.H.H., Huang, D.D., Zhou, M., Qiao, L., et al., 2020. Hourly measurements of organic molecular markers in urban Shanghai, China: observation of enhanced formation of secondary organic aerosol during particulate matter episodic periods. Atmos. Environ. 240. https://doi.org/10.1016/j.atmosenv.2020.117807.

Huang, X., Li, M., Li, J., Song, Y., 2012. A high-resolution emission inventory of crop burning in fields in China based on MODIS Thermal Anomalies/Fire products. Atmos. Environ. 50, 9–15. https://doi.org/10.1016/j.atmosenv.2012.01.017.

Isaacman, G., Kreisberg, N.M., Yee, L.D., Worton, D.R., Chan, A.W.H., Moss, J.A., et al., 2014. Online derivatization for hourly measurements of gas- and particle-phase semivolatile oxygenated organic compounds by thermal desorption aerosol gas chromatography (SV-TAG). Atmos. Meas. Tech. 7, 4417–4429. https://doi.org/10.5194/amt-7-4417-2014.

Kam, W., Liacos, J.W., Schauer, J.J., Delfino, R.J., Sioutas, C., 2012. On-road emission factors of PM pollutants for light-duty vehicles (LDVs) based on urban street driving conditions. Atmos. Environ. 61, 378–386. https://doi.org/10.1016/j.atmosenv.2012.07.072.

Kavouras, I.G., Koutrakis, P., Tsapakis, M., Lagoudaki, E., Stephanou, E.G., Von Baer, D., et al., 2001. Source apportionment of urban particulate aliphatic and polynuclear aromatic hydrocarbons (PAHs) using multivariate methods. Environ. Sci. Technol. 35, 2288–2294. https://doi.org/10.1021/es001540z.

Kotianova, P., Puxbaum, H., Bauer, H., Caseiro, A., Marr, I.L., Cik, G., 2008. Temporal patterns of n-alkanes at traffic exposed and suburban sites in Vienna. Atmos. Environ. 42, 2993–3005. https://doi.org/10.1016/j.atmosenv.2007.12.048.

Kreisberg, N.M., Hering, S.V., Williams, B.J., Worton, D.R., Goldstein, A.H., 2009. Quantification of hourly speciated organic compounds in atmospheric aerosols, measured by an in-situ thermal desorption aerosol gas chromatograph (TAG). Aerosol Sci. Technol. 43, 38–52. https://doi.org/10.1080/02786820802459583.

Leavey, A., Patel, S., Martinez, R., Mitroo, D., Fortenberry, C., Walker, M., et al., 2017. Organic and inorganic speciation of particulate matter formed during different combustion phases in an improved cookstove. Environ. Res. 158, 33–42. https://doi.org/10.1016/j.envres.2017.05.025.

Li, J.J., Wang, G.H., Wang, X.M., Cao, J.J., Sun, T., Cheng, C.L., et al., 2013. Abundance, composition and source of atmospheric PM2.5 at a remote site in the Tibetan Plateau, China. Tellus Ser. B Chem. Phys. Meteorol. 65, 16. https://doi.org/10.3402/tellusb.v65i0.20281.

Li, J., Yang, L., Gao, Y., Jiang, P., Li, Y., Zhao, T., et al., 2019a. Seasonal variations of NPAHs and OPAHs in PM2.5 at heavily polluted urban and suburban sites in North China: concentrations, molecular compositions, cancer risk assessments and sources. Ecotoxicol. Environ. Saf. 178, 58–65. https://doi.org/10.1016/j.ecoenv.2019.04.009.

Li, Q., Jiang, N., Yu, X., Dong, Z., Duan, S., Zhang, L., et al., 2019b. Sources and spatial distribution of PM2.5-bound polycyclic aromatic hydrocarbons in Zhengzhou in 2016. Atmos. Res. 216, 65–75. https://doi.org/10.1016/j.atmosres.2018.09.011.

Li, B., Zhou, S., Wang, T., Zhou, Y., Ge, L., Liao, H., 2020a. Spatio-temporal distribution and in fluencing factors of atmospheric polycyclic aromatic hydrocarbons in the Yangtze River Delta. J. Clean. Prod. 267. https://doi.org/10.1016/j.jclepro.2020.122049.

Li, R., Wang, Q., He, X., Zhu, S., Zhang, K., Duan, Y., et al., 2020b. Source apportionment of PM2.5 in Shanghai based on hourly organic molecular markers and other source tracers. Atmos. Chem. Phys. 20, 12047–12061. https://doi.org/10.5194/acp-20-12047-2020.

Lin, Y., Ma, Y., Qiu, X., Li, R., Fang, Y., Wang, J., et al., 2015. Sources, transformation, and health implications of PAHs and their nitrated, hydroxylated, and oxygenated derivatives in PM2.5 in Beijing. J. Geophys. Res.-Atmos. 120, 7219–7228. https://doi.org/10.1002/2015jd023628.

Liu, X., Zhang, Y., Cheng, Y., Hu, M., Han, T., 2012. Aerosol hygroscopicity and its impact on atmospheric visibility and radiative forcing in Guangzhou during the 2006 PRIDE-PRD campaign. Atmos. Environ. 60, 59–67. https://doi.org/10.1016/j.atmosenv.2012.06.016.

Liu, Y., Wang, S., Lohmann, R., Yu, N., Zhang, C., Gao, Y., et al., 2015. Source apportionment of gaseous and particulate PAHs from traffic emission using tunnel measurements in Shanghai, China. Atmos. Environ. 107, 129–136. https://doi.org/10.1016/j.atmosenv.2015.02.041.

Liu, Y., Yu, Y., Liu, M., Lu, M., Ge, R., Li, S., et al., 2018. Characterization and source identification of PM2.5-bound polycyclic aromatic hydrocarbons (PAHs) in different seasons from Shanghai, China. Sci. Total Environ. 644, 725–735. https://doi.org/10.1016/j.scitotenv.2018.07.049.

Liu, W., Xu, Y., Zhao, Y., Liu, Q., Yu, S., Liu, Y., et al., 2019. Occurrence, source, and risk assessment of atmospheric parent polycyclic aromatic hydrocarbons in the coastal cities of the Bohai and Yellow Seas, China. Environ. Pollut. 254. https://doi.org/10.1016/j.envpol.2019.113046.

Luo, J., He, W., Wu, J., Gu, X.S., Ye, L., 2019. Trace elements and polycyclic aromatic hydrocarbons variation along the Guang-Shen Expressway before and after the 2016 Qingming Festival in Guangzhou. Arch. Environ. Contam. Toxicol. 76, 87–101. https://doi.org/10.1007/s00244-018-0582-2.

Lyu, Y., Xu, T., Yang, X., Chen, J., Cheng, T., Li, X., 2017. Seasonal contributions to size-resolved n-alkanes (C-8-C-40) in the Shanghai atmosphere from regional anthropogenic activities and terrestrial plant waxes. Sci. Total Environ. 579, 1918–1928. https://doi.org/10.1016/j.scitotenv.2016.11.201.

Ma, L., Li, B., Liu, Y., Sun, X., Fu, D., Sun, S., et al., 2020. Characterization, sources and risk assessment of PM2.5-bound polycyclic aromatic hydrocarbons (PAHs) and nitrated PAHs (NPAHs) in Harbin, a cold city in Northern China. J. Clean. Prod. 264. https://doi.org/10.1016/j.jclepro.2020.121673.

Mehmood, T., Zhu, T., Ahmad, I., Li, X., 2020. Ambient PM2.(5) and PM10 bound PAHs in Islamabad, Pakistan: concentration, source and health risk assessment. Chemosphere 257. https://doi.org/10.1016/j.chemosphere.2020.127187.

Pehnec, G., Jakovljevic, I., Godec, R., Sever Strukil, Z., Zero, S., Huremovic, J., et al., 2020. Carcinogenic organic content of particulate matter at urban locations with different pollution sources. Sci. Total Environ. 734, 139414. https://doi.org/10.1016/j.scitotenv.2020.139414.

Ravindra, K., Bencs, L., Wauters, E., de Hoog, J., Deutsch, F., Roekens, E., et al., 2006. Seasonal and site-specific variation in vapour and aerosol phase PAHs over Flanders (Belgium) and their relation with anthropogenic activities. Atmos. Environ. 40, 771–785. https://doi.org/10.1016/j.atmosenv.2005.10.011.

Romagnoli, P., Vichi, F., Balducci, C., Imperiali, A., Perilli, M., Paciucci, L., et al., 2017. Air quality study in the coastal city of Crotone (Southern Italy) hosting a small-size harbor. Environ. Sci. Pollut. Res. 24, 25260–25275. https://doi.org/10.1007/s11356-017-0126-8.

Ronkko, T.J., M-R, Hirvonen, Happo, M.S., Leskinen, A., Koponen, H., Mikkonen, S., et al., 2020. Air quality intervention during the Nanjing Youth Olympic Games altered PM sources, chemical composition, and toxicological responses. Environ. Res. 185. https://doi.org/10.1016/j.envres.2020.109360.

Sachdeva, K., Attri, A.K., 2008. Morphological characterization of carbonaceous aggregates in soot and free fall aerosol samples. Atmos. Environ. 42, 1025–1034. https://doi.org/10.1016/j.atmosenv.2007.10.002.

Sak, Z.H.A., Kurtulus, S., Ocakli, B., Toreyin, Z.N., Bayhan, I., Yesilnacar, M.I., et al., 2018. Respiratory symptoms and pulmonary functions before and after pesticide application in cotton farming. Ann. Agric. Environ. Med. 25, 701–707. https://doi.org/10.26444/aaem/99561.

Scalan, E.S., Smith, J.E., 1970. An improved measure of the odd-even predominance in the normal alkanes of sediment extracts and petroleum. Geochim. Cosmochim. Acta 34, 611–620. https://doi.org/10.1016/0016-7037(70)90019-0.

Schauer, J.J., Kleeman, M.J., Cass, G.R., Simoneit, B.R.T., 2002. Measurement of emissions from air pollution sources. 5. C-1-C-32 organic compounds from gasoline-powered motor vehicles. Environ. Sci. Technol. 36, 1169–1180. https://doi.org/10.1021/es0108077.

Shimada, K., Nohchi, M., Yang, X., Sugiyama, T., Miura, K., Takami, A., et al., 2020. Degradation of PAHs during long range transport based on simultaneous measurements at Tuoji Island, China, and at Fukue Island and Cape Hedo, Japan. Environ. Pollut. 260, 113906. https://doi.org/10.1016/j.envpol.2019.113906.

Su, P., Zhang, W., Hao, Y., Tomy, G.T., Yin, F., Chen, L., et al., 2020. Polycyclic aromatic hydrocarbon contaminations along shipping lanes and implications of seafarer exposure: based on PAHs in ship surface films and a film -air -water fugacity model. Sci. Total Environ. 731. https://doi.org/10.1016/j.scitotenv.2020.138943.

Sun, T., Che, H., Qi, B., Wang, Y., Dong, Y., Xia, X., et al., 2019. Characterization of vertical distribution and radiative forcing of ambient aerosol over the Yangtze River Delta during 2013–2015. Sci. Total Environ. 650, 1846–1857. https://doi.org/10.1016/j.scitotenv.2018.09.262.

Teixeira, E.C., Agudelo-Castaneda, D.M., Guimaraes Fachel, J.M., Leal, K.A., KdO, Garcia, Wiegand, F., 2012. Source identification and seasonal variation of polycyclic aromatic hydrocarbons associated with atmospheric fine and coarse particles in the Metropolitan Area of Porto Alegre, RS, Brazil. Atmos. Res. 118, 390–403. https://doi.org/10.1016/j.atmosres.2012.07.004.

Vasilakos, C., Levi, N., Maggos, T., Hatzianestis, J., Michopoulos, J., Helmis, C., 2007. Gasparticle concentration and characterization of sources of PAHs in the atmosphere of a suburban area in Athens, Greece. J. Hazard. Mater. 140, 45–51. https://doi.org/10.1016/j.jhazmat.2006.06.047.

Wang, Y.Q., Zhang, X.Y., Draxler, R.R., 2009. TrajStat: GIS-based software that uses various trajectory statistical analysis methods to identify potential sources from long-term air pollution measurement data. Environ. Model. Softw. 24, 938–939. https://doi.org/10.1016/j.envsoft.2009.01.004.

Wang, F., Lin, T., Feng, J., Fu, H., Guo, Z., 2015. Source apportionment of polycyclic aromatic hydrocarbons in PM2.5 using positive matrix factorization modeling in Shanghai, China. Environ. Sci. Process. Impacts 17, 197–205. https://doi.org/10.1039/c4em00570h.

Wang, F., Guo, Z., Lin, T., Rose, N.L., 2016a. Seasonal variation of carbonaceous pollutants in PM2.5 at an urban 'supersite' in Shanghai, China. Chemosphere. 146, 238–244. https://doi.org/10.1016/j.chemosphere.2015.12.036.

Wang, Q., Feng, Y., Huang, X.H.H., Griffith, S.M., Zhang, T., Zhang, Q., et al., 2016b. Nonpolar organic compounds as PM2.5 source tracers: investigation of their sources and degradation in the Pearl River Delta, China. J. Geophys. Res.-Atmos. 121, 11862–11879. https://doi.org/10.1002/2016jd025315.

Wang, F., Lin, T., Li, Y., Guo, Z., Rose, N.L., 2017. Comparison of PM2.5 carbonaceous pollutants between an urban site in Shanghai and a background site in a coastal East China Sea island in summer: concentration, composition and sources. Environ. Sci. Process. Impacts 19, 833–842. https://doi.org/10.1039/c7em00129k.

Wang, M., R-J, Huang, Cao, J., Dai, W., Zhou, J., Lin, C., et al., 2019. Determination of n-alkanes, polycyclic aromatic hydrocarbons and hopanes in atmospheric aerosol: evaluation and comparison of thermal desorption GC-MS and solvent extraction GC-MS approaches. Atmos. Meas. Tech. 12, 4779–4789. https://doi.org/10.5194/amt-12-4779-2019.

Wang, Q.Q., He, X., Zhou, M., Huang, D.D., Qiao, L.P., Zhu, S.H., Ma, Y.G., Wang, H.L., Li, L., Huang, C., Huang, X.H., Xu, W., Worsnop, D., Goldstein, A.H., Guo, H., Yu, J.Z., 2020. Hourly measurements of organic molecular markers in urban Shanghai, China: primary organic aerosol source identification and observation of cooking aerosol aging. ACS Earth Space Chem. 1670−1685, 4. https://doi.org/10.1021/acsearthspacechem.0c00205.

Williams, B.J., Goldstein, A.H., Kreisberg, N.M., Hering, S.V., 2006. An in-situ instrument for speciated organic composition of atmospheric aerosols: thermal desorption aerosol GC/MS-FID (TAG). Aerosol Sci. Technol. 40, 627–638. https://doi.org/10.1080/02786820600754631.

Wiriya, W., Chantara, S., Sillapapiromsuk, S., N-H, Lin, 2016. Emission profiles of PM10-bound polycyclic aromatic hydrocarbons from biomass burning determined in chamber for assessment of air pollutants from open burning. Aerosol Air Qual. Res. 16, 2716–2727. https://doi.org/10.4209/aaqr.2015.04.0278.

Wu, J., Kong, S., Wu, F., Cheng, Y., Zheng, S., Yan, Q., et al., 2018. Estimating the open biomass burning emissions in central and eastern China from 2003 to 2015 based on satellite observation. Atmos. Chem. Phys. 18.

Xu, T., Lv, Y., Cheng, T., Li, X., 2015. Using comprehensive GCxGC to study PAHs and n-alkanes associated with PM2.5 in urban atmosphere. Environ. Sci. Pollut. Res. 22, 5253–5262. https://doi.org/10.1007/s11356-014-3695-9.

Yan, C., Zheng, M., Yang, Q., Zhang, Q., Qiu, X., Zhang, Y., et al., 2015. Commuter exposure to particulate matter and particle-bound PAHs in three transportation modes in Beijing, China. Environ. Pollut. 204, 199–206. https://doi.org/10.1016/j.envpol.2015.05.001.

Yan, D., Wu, S., Zhou, S., Tong, G., Li, F., Wang, Y., et al., 2019. Characteristics, sources and health risk assessment of airborne particulate PAHs in Chinese cities: a review. Environ. Pollut. 248, 804–814. https://doi.org/10.1016/j.envpol.2019.02.068.

Yang, F., Zhai, Y., Chen, L., Li, C., Zeng, G., He, Y., et al., 2010. The seasonal changes and spatial trends of particle-associated polycyclic aromatic hydrocarbons in the summer and autumn in Changsha city. Atmos. Res. 96, 122–130. https://doi.org/10.1016/j.atmosres.2009.12.004.

Yang, L., Zhang, X., Xing, W., Zhou, Q., Zhang, L., Wu, Q., et al., 2021. Yearly variation in characteristics and health risk of polycyclic aromatic hydrocarbons and nitro-PAHs in urban shanghai from 2010–2018. J. Environ. Sci. (China) 99, 72–79. https://doi.org/10.1016/j.jes.2020.06.017.

Yi, Y.-n., Hou, Z-f, Yang, Q.-c, Liu, X-d, Li, Z., Meng, J-j., et al., 2020. Chemical compositions and sources of n-alkanes and saccharides in PM2.5 from Taian City during the summer. Environ. Sci. 41, 1045–1055 (in Chinese). 10.13227/j.hjkx.201907070.

Zhang, Q., Jimenez, J.L., Canagaratna, M.R., Allan, J.D., Coe, H., Ulbrich, I., et al., 2007. Ubiquity and dominance of oxygenated species in organic aerosols in anthropogenically-influenced Northern Hemisphere midlatitudes. Geophys. Res. Lett. 34. https://doi.org/10.1029/2007gl029979.

Zhang, K., Li, L., Huang, L., Wang, Y., Huo, J., Duan, Y., et al., 2020a. The impact of volatile organic compounds on ozone formation in the suburban area of Shanghai. Atmos. Environ. 232. https://doi.org/10.1016/j.atmosenv.2020.117511.

Zhang, L., Xu, H., Fang, B., Wang, H., Yang, Z., Yang, W., et al., 2020b. Source identification and health risk assessment of polycyclic aromatic hydrocarbon-enriched PM2.5 in Tangshan, China. Environ. Toxicol. Chem. 39, 458–467. https://doi.org/10.1002/etc.4618.

Zhao, Y., Hu, M., Slanina, S., Zhang, Y., 2007a. Chemical compositions of fine particulate organic matter emitted from Chinese cooking. Environ. Sci. Technol. 41, 99–105. https://doi.org/10.1021/es0614518.

Zhao, Y., Hu, M., Slanina, S., Zhang, Y., 2007b. The molecular distribution of fine particulate organic matter emitted from Western-style fast food cooking. Atmos. Environ. 41, 8163–8171. https://doi.org/10.1016/j.atmosenv.2007.06.029.

Zhao, Y., Kreisberg, N.M., Worton, D.R., Isaacman, G., Weber, R.J., Liu, S., et al., 2013. Insights into secondary organic aerosol formation mechanisms from measured gas/particle partitioning of specific organic tracer compounds. Environ. Sci. Technol. 47, 3781–3787. https://doi.org/10.1021/es304587x.

Zhao, Y., Chen, C., Zhao, B., 2019. Emission characteristics of PM2.5-bound chemicals from residential Chinese cooking. Build. Environ. 149, 623–629. https://doi.org/10.1016/j.buildenv.2018.12.060.